MICROSTUCTURE AND MACROSTRUCTURE

Gregory S. Rohrer

Department of Materials Science and Engineering

Carnegie Mellon University

Pittsburgh, PA 15213, USA

Introduction

A crystalline solid is made up of indistinguishable groups of atoms positioned at the sites of a Bravais lattice. If the atomic structure is approximately uniform in both orientation and composition throughout the solid, the material is referred to as a single crystal. When the atomic structure is not uniform, it is known as a polycrystal. In this second and more common instance, the irregularities in the orientation, composition, and configuration of the atomic structure collectively make up what is referred to as the internal structure or microstructure. The term macrostructure is sometimes used to refer to the largest components of the internal structure. Within this article, all components of the internal structure will be referred to as the microstructure.

Polycrystals can be thought of as aggregates of much smaller crystals joined together by a network of internal interfaces, as illustrated schematically in Fig. 1. Within the aggregate, the individual crystals are referred to as grains. The interface that separates two grains of the same composition, but different lattice orientation, is called a grain boundary and the interface that separates two grains with different compositions is called a phase boundary. The granular nature of polycrystalline matter has been recognized since at least 1775 when Grignon sketched grains observed on the surface of a piece of fractured wrought iron. This first recorded observation points to an important feature of the interfaces within the microstructure: they are frequently points of internal

weakness along which failure, by fracture or corrosion, propagates through the interfacial network. During the last century, microstructural studies have flourished amid the realization that many of the macroscopic properties of polycrystalline solids are strongly influenced by the internal structure. While these studies established the solid foundation of knowledge that will be reviewed in this article, it should also be recognized that there are many unresolved questions about microstructural genesis and the microstructure-property link that continue to be actively researched. In general terms, one can say that polycrystalline microstructures results from crystal nucleation, growth, and capillarity driven morphological changes that lead to a reduction in the interfacial energy. In this article, the basic principles behind these processes will be described and examples of prototypical microstructures will be presented. The article will focus on dense, inorganic, polycrystalline microstructures that occur in man-made materials. Single phase microstructures are discussed first and multiphased structures are described in the second section.

Single Phase Microstructures

The term single phase polycrystal is used to described an aggregate of crystals that is uniform in its atomic structure and composition. Throughout a single phase microstructure, it is only the orientation of the Bravias lattice within the individual grains that differs. The defining elements of the microstructure are the distribution of crystal sizes, the distribution of crystal shapes, the distribution of crystal orientations, and the types of grain boundaries between the crystals. Single phase microstructures can be formed by sintering a solid powder, by crystallizing a precursing liquid, gaseous, or

amorphous phase, or by recrystallizing a deformed precursor. Microstructures resulting from each of these states are described briefly below.

Single phase microstructures by sintering

The excess free energy per unit area of a grain boundary (γ) can be thought of as the energy to create equal areas of the two free surfaces on either side of the boundary, minus a binding energy associated with the formation of bonds across the interface as the surfaces are joined. Therefore, as long as there is bonding across the interface, it is energetically preferable to replace two free surfaces with a grain boundary of the same area. This is the driving force for the process of sintering, in which individual crystalline particles change shape and bond with one another to form a dense polycrystal. Further heating after complete densification leads to grain growth, an increase in the average grain size. This too is a capillarity driven process, because as the average grain size increases, the total grain boundary area (and its associated energy) decreases. If the grain boundary energy and mobility are not too anisotropic, then an equiaxed microstructure develops. In other words, each grain has approximately the same dimensions in all directions. An equiaxed microstructure is illustrated in Fig. 2.

The shapes of the grains are determined in part by the relative rates at which the crystal grows in different directions (a kinetic effect), and in part by the requirement that the interfacial forces balance at their points of intersection (an equilibrium effect). The equilibrium equation for the point where three interfaces meet is known as the Herring condition:

$$\sum_{i=1 \text{ to } 3} \gamma_i \mathbf{t}_i + \frac{\partial \gamma_i}{\partial \beta_i} \mathbf{n}_i = \mathbf{0}$$

The terms in this expression are described in Fig. 3. Under the condition that the energy does not depend on orientation, this reduces to the more familiar Young equation,

$$\frac{\gamma_1}{\sin\Psi_1} = \frac{\gamma_2}{\sin\Psi_2} = \frac{\gamma_3}{\sin\Psi_3}$$

where the Ψ_i are the dihedral angles in Fig. 3. If the energies of all the interfaces are assumed to be equal, then all of the dihedral angles are 120°. If this is the case, then dihedral angles at quadrajunctions where four triple lines intersect must be 109.5°. To meet these conditions and fill space, some curvature must be introduced in the boundaries and this creates a driving force for motion. Boundaries always move toward their center of curvature to reduce their total area. The situation was considered in two-dimensions by von Neumann and Mullins, who showed that if equilibrium dihedral angles are to be maintained in an isotropic structure, then grains with more than six sides will always grow and grains with fewer than six sides will shrink (see Fig. 4). While the problem is not easily solved in three dimensions, it is currently thought that grains with 13 or fewer faces shrink while those with 14 or more grow. Studies of three dimensional shapes are consistent with this criterion. In a variety of studies, the average number of faces per grain has been measured to be between 12 and 14. A sketch of a typical grain is shown in Fig. 5.

Kinetic grain growth theories generally predict that the average grain size increases with the square root of time (t) so that the average radius, <r>, is:

$$\langle r \rangle = (Kt)^n$$

Where K is a positive constant and n, the grain growth exponent, is ideally equal to 1/2.

Furthermore, after the effects of the initial grain size distribution have disappeared, there

is a steady state distribution of grain sizes that is scale invariant. The form of the

distribution, originally derived by Hillert, has a maximum grain size that is about 3/2

times the average size:

$$P_H(\rho) = (2e)^3 \frac{3\rho}{(2-\rho)^5} \exp[-6/(2-\rho)]$$

In this equation, $\rho = r/r^*$, where r^* is the critical radius; grains smaller than r^* shrink

while grains larger than r^* grow. The distribution is plotted in Fig. 6. In practice,

observed grain growth exponents are usually less than 1/2, the maximum grain size

greatly exceeds 3/2 times the average, and the distribution of grain sizes is most

frequently reported to be lognormal, where the number of grains with dimensionless size

ρ is:

$$P_L(\rho) = \frac{1}{\sqrt{2\pi}\sigma} \frac{1}{\rho r^*} \exp\left[-(\ln\rho)^2/2\sigma^2\right]$$

In this expression, σ is the width of the distribution. Microstructures that exhibit

unimodal and roughly lognormal distributions of grain sizes are usually called normal.

However, in some cases the distribution of grain sizes is bimodal (see Fig. 6 for

comparison to normal distributions) and such distributions are said to be the result of abnormal growth. An example of a microstructure with an abnormal distribution of grain sizes is illustrated in Fig. 7.

When the anisotropy in the grain boundary energy and mobility is large, the grains adopt distinct shapes and are frequently bounded by flat interfaces, indicating that the orientation corresponds to a cusp or singularity in the function that describes the orientation dependence of the grain boundary energy. For example, the microstructure in Fig. 8 shows a section through randomly oriented plate-like grains. Depending on the processing, the shapes may also exhibit preferred orientation or texture, as illustrated in Fig. 9. In this case, the [0001] axes of the rhombohedral lattice of Al_2O_3 are oriented in the vertical direction. The general phenomena of nonrandom distributions of crystal orientations with respect to the external reference frame, as illustrated in Fig. 9, is referred to as texture.

Single phase microstructures by crystallization

When a microstructure forms by crystallization from a liquid, gas, or amorphous matrix, crystal nucleation requires the formation of an interface between the crystalline and noncrystalline phase. Assuming that the interface energy (γ_s) is isotropic and that the change in free energy per volume upon crystallization is ΔG_v, then the free energy change for the formation of a nucleus with radius r is given by

$$\Delta G(r) = 4\pi r^2 \gamma_s - \frac{4}{3}\pi r^3 \Delta G_v$$

As illustrated in Fig. 10, the change in the free energy as a function r is initially positive.
Only after a critical size is reached will further growth stabilize the crystal. Thus, there is
an energy barrier, ΔG^*, that inhibits homogeneous nucleation. If a heterogeneous surface
is present (for example, the mould walls of a casting system or a substrate in a vapor
deposition system), and there almost always is, then we have to consider not only the
creation of the surface dividing the nucleus from the surrounding liquid or gas, but also
the elimination of the heterogeneous surface and the creation of the interface between the
nucleus and the heterogeneous surface. Using the Young equation, the relationship
between the various interface energies can be expressed as a contact angle, θ, in the
following way:

$$cos\theta = \frac{(\gamma_h - \gamma_{sh})}{\gamma_s}$$

The terms in the equation above are defined in the Fig. 10, assuming the crystallization of
a spherical cap on the heterogeneous surface. With this parameter, the free energy
change for heterogeneous nucleation can be written in a form similar to that for
homogeneous nucleation:

$$\Delta G(r) = \left[4\pi r^2 \gamma_s - \frac{4}{3}\pi r^3 \Delta G_v \right] S(\theta)$$

Where the shape factor is $S(\theta)=(2+cos\theta)(1-cos\theta)^2/4$. Since this term is always less than
unity, the free energy change for heterogenous nucleation is always less than that for

homogeneous nucleation. Thus, crystal formation always initiates from a heterogeneity

and most frequently from the walls of the container or a deliberately introduced substrate.

This leads to so-called columnar microstructures, such as those illustrated in Figs. 11 and

12. The microstructure in Fig. 11 results from nucleation and growth from the walls of a

mould in a casting and the microstructure in 12 results from the deposition of a vapor on

a substrate. It should be recognized that heterogeneous nucleation can be initiated in a

more or less uniform manner by introducing a finely dispersed heterogeneity and this can

lead to a equiaxed microstructure. Uniform heterogeneous nucleation can also occur

when a material is recrystallized from a deformed matrix.

Grain boundaries in single phase microstructures

The complexity of the grain boundary networks within polycrystals arises from

the number of crystallographic degrees of freedom. Three parameters are required to

describe the lattice misorientation between two crystals and two additional parameters are

required to describe the orientation of the grain boundary plane. The number of

distinguishable boundary types in this five dimensional parameter space is large. For

example, in a cubic material, if the five parameters are measured with 5° of resolution,

then there are 5×10^4 distinguishable types of grain boundaries. In general, the

distribution of grain boundary surface area is not uniform over the five parameters.

Textures have been measured both in the space of lattice misorientations and grain

boundary orientations. For example, Fig. 13 shows the distribution of lattice

misorientations in WC, showing that boundaries with a 30 ° misorientation about [0001]

and a 90 ° misorientation about [10$\bar{1}$0] occur with a higher and random frequency.

These data are plotted without regard for the particular boundary plane. In Fig. 14, the

distribution of grain boundary plane area is shown for the two highly populated

misorientations identified in Fig. 13.   These data demonstrate that hexagonal WC has a

preference for grain boundary planes terminated on $\{0001\}$ and $\{10\bar{1}0\}$ surfaces.

   While the mechanistic origin of the grain boundary texture is not yet understood,

it is known that the frequency with which different grain boundaries occur in a

polycrystal is inversely related to the energy. Those boundaries with low energies or

some other extraordinary property are thought to be especially influential in determining

macroscopic properties. One such boundary is a twin. Twins in different materials have

different crystallographic parameters, but the common feature is that they have a well

defined lattice misorientation and habit plane that allows the atoms within the interface to

occupy positions that are very similar to those of the bulk. For example, in a cubic close

packed metal, a boundary formed between two crystals whose (111) planes are parallel,

but rotated by 60 ° around the vector perpendicular to the boundary planes, is a twin.

This particular boundary is only a minor disruption in the long range structure and is

indistinguishable from a stacking fault. All of the atoms in the boundary plane still have

12 nearest neighbors in the same pattern; it is only the configuration of the next near

neighbors that differs. This special condition occurs only on this one plane, so it is

energetically very costly to rotate this boundary away from the (111) orientation. While

the crystallography varies from system to system, this is a common feature and as a

result, twins are very flat, planar boundaries without noticeable curvature. Because a

twin has a low energy, the dihedral angle it makes with other more general grain

boundaries is usually very close to 180 °. These are the geometric characteristics that

make twins easy to locate in a microstructure.

In cubic close packed metals, twins commonly form during recrystallization. An example of a highly twined alpha brass microstructure is illustrated in Fig. 15. In tetragonal materials, if there is only a small difference between the **a** and **c** lattice parameters, then mosaic twinning in common. A twinned $BaTiO_3$ structure is illustrated in Fig. 16 (this is a higher resolution image of the twins that were evident in Fig. 7). This material has a tetragonally distorted perovskite structure with a **c** to **a** ratio of 1.01. The straight boundaries all correspond to 90 °!rotations about a <100> axis with the boundary on a {110} plane.

Boundaries with misorientations that place a high fraction of lattice sites in coincidence are also distinguished from more general boundaries. These boundaries are called coincident site lattice boundaries and are assigned a coincidence number (Σ) based on the inverse of the number of coincident lattice sites. Therefore, a low Σ number signifies high coincidence. For example, illustrations of the $\Sigma5$ and $\Sigma13$ boundaries are presented in Fig. 17. In many circumstances, boundaries of high coincidence are also referred to as "special" boundaries, although the term is not always used in a consistent manner. Note that while the coincidence relation depends only on the lattice misorientation, high coincidence is only achieved if the boundary lies on certain planes where the lattice sites overlap. Therefore, of all boundaries with a low Σ misorientation, only those with the interface planes oriented in a specific direction are expected to have special properties. The twin in the cubic close packed system a good example. This corresponds to a boundary with a 60° misorientation about the [111] axis, with the boundary on a (111) plane. The designation $\Sigma3$ refers to the same misorientation, but does not specify the boundary plane.

Boundaries with low Σ misorientations have recently taken on a special significance because it has been found that certain materials properties are improved by increasing the fraction of these low Σ boundaries, particularly those known as $\Sigma3^n$, including $\Sigma3$, $\Sigma9$, and $\Sigma27$. In cubic close packed materials with low stacking fault energies, such as Cu, Ni, and Pb, the fractional population of $\Sigma3^n$ boundaries can be increased by the process referred to as grain boundary engineering. In this process, the materials undergo repeated cycles of mild deformation followed by recrystallization. After each cycle, the concentration of $\Sigma3^n$ boundaries increases. The micrograph in Fig. 15, discussed above, shows an example of a grain boundary engineered microstructure in which approximately 45 % of the boundaries are of the type $\Sigma3^n$. As the special boundaries increase in concentration, they break up percolating clusters of general boundaries that are more susceptible to failure.

Duplex Microstructures

Duplex microstructures contain two distinct phases, which are materials that can be distinguished on the basis of structure or composition. In principle, a microstructure may contain many different phases, but the discussion here is limited to the case of two phases. The defining elements of the two-phase microstructure are the same as in the single phase microstructure, only it is also necessary characterize the configuration of the two phases and the volume fractions. As in the single phase microstructures, the configuration is determined both by equilibrium phenomena and kinetic phenomena. Because of the added complexity, there are a wider range of possibilities. Selected cases are discussed in the following sections.

Duplex microstructures formed by consolidation

The most direct method to create a duplex microstructure is to physically mix the two phases and then consolidate the mixture by sintering. The degree to which the two phases wet each other strongly influences the configuration. Referring once again to the Young equation, the equilibrium geometry at the points where the phases meet is a function of the interfacial energies. If we label the phases A and B, and assume that their interface energies are isotropic, then the dihedral angle between the two AB interfaces (see Fig. 18) is given by:

$$\cos(\Psi) = \gamma_{AA}/2\gamma_{AB}$$

Note that when $2\gamma_{AB} << \gamma_{AA}$, the dihedral angle goes to zero and in this case the two phases completely wet each other. As γ_{AB} approached γ_{AA}, the two phases become increasing non-wetting and the dihedral angle increases toward 180°. Two examples are shown in Fig. 19 and 20. In Fig. 19, Co, which is liquid at the processing temperature, completely wets the angular WC crystals. In this case, the WC crystals occupy 90 % of the volume and form an interconnected, skeletal network. The aluminum oxide - tanatalum oxide mixture in Fig. 20 provides an example of a non-wetting combination. The dark grains are the Al-rich phase which poorly wets the Ta_2O_5 boundaries.

Duplex microstructures by solidification

When microstructures form by the solidification of a homogeneous liquid, the phases are not as uniformly dispersed as when formed by a physical mixture followed by

consolidation. Interestingly, well defined patterns can develop under these conditions.

When a single phase liquid is crystallized in a two phase region where a solid and liquid

phase coexist, one of the most common morphological patterns to develop is the dendrite,

or branched structure, as illustrated by the microstructures in Fig. 21 and 22. It should be

noted that while dendrites can also form during the solidification of a pure material into a

supercooled liquid, this situation is far less common than that of the binary alloy. For the

single phase case, one can imagine that protrusions in the growth front can be stabilized if

the liquid is supercooled and the latent heat of crystallization is extracted through the

solid. In this case, heat is removed more efficiently from the tip of the protrusion that

juts out into the supercooled fluid than it is from the valleys between protrusions.

To described the mechanism by which dendrites form in a binary alloy, consider

the simple binary eutectic phase diagram illustrated in Fig. 23. For an alloy with

composition C at a temperature less than T_L, there is a range of temperature where the

solid and liquid coexist, but with different compositions. The solid alloy α has

composition C_α and always contains less B than the liquid, with composition C_L. In fact,

one can say that the solid is always relatively more pure than the liquid from which it

crystallizes. This means that as the crystal grows, the liquid at the interface is relatively

enriched in B and that the enriched liquid freezes at a lower temperature, specified by the

liquidus line in Fig. 23. Therefore, a protrusion in the interface can be stabilized because

it juts into a relatively more pure liquid (see Fig. 24). In the valleys between protrusions,

on the other hand, the liquid rich in B is trapped between opposing growth fronts. Thus,

the growth front at the tip of the protrusion is in contact with a liquid that freezes at a

higher temperature than the liquid in the valleys between the protrusions. This causes the

tip to grow faster than the lateral surfaces and the result is cellular or, more commonly, a dendritic morphology

When the remaining liquid cools to the temperature T_E, two solid phases (α and β) crystallize directly from the liquid. This most frequently results in a lamellar microstructure, such as those shown in Fig. 25, where the two phases have alternating bands of dark and light contrast. Because both solids are in equilibrium with the same liquid, but themselves have very different compositions, they must simultaneously reject solute to feed the growth of the other phase. In other words, as a layer of the α phase grows, it must reject solute (B) laterally to supply neighboring lamella of the β phase. As the β phase crystallizes, it rejects A, which sustains the growth of the α phase. This cooperative process, schematically illustrated in Fig. 26, stabilizes a nearly planar growth front.

In most solidification processes, cooling will take the materials through a region of solid-liquid coexistence, in which a dendritic structure will grow. When the remaining liquid reaches the eutectic temperature, it will solidify in a lamellar microstructure, leading to a mixed microstructure. In general, this situation is not an equilibrium configuration. Annealing at a temperature just below the eutectic will cause the compositional concentration gradients to homogenize and the morphologies of the crystals to spheroidize and become more equiaxed.

Duplex microstructures by Transformation in the solid phase

Duplex microstuctures can also form by transformation in the solid phase. As an example, consider the rapid cooling of α on the phase diagram in Fig. 23, from T_s to T_{ss}.

At T_{ss}, the supersaturated a phase will decompose to $\alpha+\beta$, and this will happen entirely in the solid state. As with solidification, the characteristics of the microstructure that develop are determined by the nucleation and growth of the phase. The free energy change during the nucleation process is similar to that for heterogeneous nucleation, except that an additional term must be added to account for the volumetric strain energy associated with any expansion or contraction that might accompany the transformation. The disposition and shape of this phase depends on the structural relationship between the parent and daughter phases, features preexisting in the microstructure that serve as heterogeneous nucleation sites, the degree of supersaturation during the nucleation and growth of the phase, and the mechanism of the transformation. Because of all of these parameters, there are a wide range of possible microstructures that can form and only a few of characteristic examples are described in the remainder of this article.

Precipitation from a supersaturated solid solution requires the long range diffusion of solute to the site of growth. For this reason, the distribution of a precipitated phase will depend in the degree of undercooling or supersaturation. When large, the driving force for the precipitation reaction is amplified and atomic mobility is limited. This leads of a uniform distribution of very small precipitates. For example, the microstructure in Fig. 27 shows cuboidal γ' precipitates in a $Ni_{70}Cr_{20}Al_{10}$ superalloy. In this case, the structure of precipitating phase differs little from that of the parent phase, so there is an orientation relationship between the two. In cases where the kinetics for transport are higher and the supersaturation is not as large, precipitates will nucleate at heterogeneities such as grain boundaries.

The formation of lamellar microstructures from the solidification of a eutectic has already been described. In the case of the eutectoid reaction, where a single solid phase decomposes to two new solid phases, the microstructure that is formed is similar to that formed by the eutectic reaction, but the lamellar phase typically nucleates and grows from the grain boundaries. Similar microstructures can also be generated by the cellular transformation from a supersaturated solid solution.

There are also solid to solid transformations that do not require long range diffusion and these processes also lead to distinct microstructures. In the massive transformation, a single phase decomposes to one or more phases that have the same composition, but different crystal structures. Because it is not necessary to alter the composition, the interface can move very rapidly. The massive transformation frequently nucleates at grain boundaries and the rapid interface motion leaves an irregularly shaped precipitate. Ordering transformations can also occur with very little long range diffusion. In this case, elements A and B originally occupy certain sites in the crystal structure at random. Below a certain temperature, they occupy the same sites, but in an ordered fashion, as illustrated schematically in Fig. 28. Because the ordering process will begin in many places at once, impingement will create antiphase domain boundaries, where there is a shift in the ordering pattern. A characteristic microstructure with APBs is illustrated in Fig. 29.

Martensitic transformations are diffusionless processes by which a material changes crystal structure without requiring any of the atoms to change position by more than a lattice spacing. Typically, the parent and daughter structure are related by a shear deformation process. In the resulting microstructure, lens shaped precipitates grow

quickly to the size of the grains of the parent phase, creating the characteristic microstructure, such as the one illustrated in Fig. 7, where the twins within the grains have formed by a martinsitic transformation. It has been shown that the interface between the precipitate and the parent phase can move at velocities approaching the speed of sound.

Bibliography

Bunge H-J (1982) *Texture Analysis in Materials Science*, Translated by P.R Morris. London, U.K., Butterworths.

Burton WK, Cabrera N, Frank FC (1951) The Growth of Crystals and the Equilibrium Structure of Their Surfaces, *Philos. Trans. R. Soc. London, Ser. A*, Vol. 243, pp. 300-58.

Herring C (1951) Surface Tension as a Motivation for Sintering. In: Kingston WE (ed) *The Physics of Powder Metallurgy*, pp. 143-79. McGraw Hill, New York.

Hillert M (1965) On the Theory of Normal and Abnormal Grain Growth, *Acta Met*. Vol. 13, pp. 227-38.

(1985) Metallography and Microstructures, *Metals Handbook*, 9th edn, American Society of Metals, Metals Park, OH.

Mullins WW (1956) Two Dimensional Motion of Idealized Grain Boundaries, *J. Appl. Phys*. Vol. 27, 900-904.

Mullins WW and Sekerka RF (1964) Stability of a Planar Interface During Solidification of a Dilute Binary Alloy, *J. Appl. Phys*. Vol. 35, pp. 444-451.

Porter DA, Easterling KE (1981) Phase Transformations in Metals and Alloys, London, Chapman Hall.

Randle (1996) *The role of the Coincident Site Lattice in Grain Boundary Engineering*. Institute of Materials, London.

Rohrer GS, Saylor DM, El-Dasher BS, Adams BL, Rollett AD, Wynblatt P (2004) The Distribution of Internal Interfaces in Polycrystals, *Zeitschrift fur Metallkunde* Vol. 95 pp. 1-18.

Smith CS (1952) The Shapes of Metal Grains, with some Other Metallurgical Applications of Topology. In: *Metal Interfaces*, p. 65. ASM. Cleveland 1952.

Smith CS (1964) Some Elementary Principles of Polycrystalline Microstructure, *Metal. Rev*. vol. 9, pp. 1-48.

Smith CS (1981) *A Search for Structure*. MIT Press, Cambridge, MA, 1981.

Tiller WA (1991) The Science of Crystallization: Macroscopic Phenomena and Defect Generation. Cambridge University Press, Cambridge.

Figures

Figure 1. Schematic illustration of a polycrystalline solid, with black dots representing points on the lattice and gray lines denoting boundaries between grains with different orientations.

Figure 2. Montage of scanning electron microscope (SEM) images of spinel, $MgAl_2O_4$. The contrast at the grain boundaries results from thermal grooving.

Figure 3. Schematic of the triple line (**l**) along which three interfaces meet, defining the terms in the Herring equation.

Figure 4. Schematic showing the configurations of boundaries in a two dimensional system under the assumption that the grain boundary energy is isotropic. In this case, the boundaries must always meet with 120° dihedral angles. This means that if a grain has fewer than six sides, the boundaries are convex and will move inward (a and b), if it has exactly six sides there is no curvature and the boundaries are stationary (c) and if it has more than six sides (d) the boundaries are concave and move outward.

Figure 5. A schematic showing the three dimensional shape of a grain within a polycrystal. The black lines are edges on the front of the grain and the gray lines are edges on the back of the grain.

Figure 6. Grain size distributions. The most commonly observed distribution of grain sizes is lognormal (P_L) while the theory of capillary driven grain growth predicts a different distribution (P_H). A schematic of a bimodal distribution is shown in the lower part of the figure.

Figure 7. Visible light micrograph showing the microstructure of a polycrystalline $BaTiO_3$ specimen. Parts of two grains on the left are much larger than the cluster of average grains on the right. The regular patterns within each grain are twin plates that formed by a martinsitic transformation during cooling.

Figure 8. Atomic force microscope image of polycrystalline $Sr_2Nb_2O_7$. The orthorhombic material has platy grains elongated along the **a** and **c** axes.

Figure 9. SEM micrograph of a tabular alumina microstructure formed by templated grain growth. The short dimension of the crystal is oriented along the [0001] axis. Micrograph courtesy of Gary L. Messing and Matthew M. Seabaugh, Department of Materials Science and Engineering, Pennsylvania State University.

Figure 10. Plot of the free energy change as a function of nucleus radius. The change is initially positive. Additional growth reduces the energy only beyond a critical size. For heterogeneous nucleation, the barrier is lower.

Figure 11. Section through a cylindrical casting. The elongated grains nucleated on the mould walls (top and bottom of the micrograph) and grew toward the center. Micrograph courtesy of H.P. Paxton, Department of Materials Science and Engineering, Carnegie Mellon University.

Figure 12. Columnar thin film multilayer microstructure. The NiAl grains nucleated on the Ni-P layer and the columnar structure is maintained through the Co and Cr layers. Micrograph courtesy of David E. Laughlin, Department of Materials Science and Engineering, Carnegie Mellon University.

Figure 13. The grain boundary character distribution in WC, plotted in axis-angle space. The entire range of distinguishable misorienation axes in the hexagonal system is represented in each triangle, and the individual triangles represent different rotations about these axes. The units are in multiples of a random distribution (MRD).

Figure 14. The distribution of grain boundary planes at two specific misorientations: (a) for 90 ° rotations about the $[10\bar{1}0]$ axis and (b) 30 ° about the [0001] axis. The hexagon marks to position of the [0001] axis and the rectangle the position of the [1000] axis. The

positions of the peaks indicate that for both types of grain boundaries, the pure twist

configuration is preferred.

Figure 15. Image quality electron backscattered pattern map of alpha brass. The black

lines indicate the positions of grain boundaries. The straight boundaries are twins.

Micrograph courtesy of Valerie Randle, University of Wales, Swansea.

Figure 16. AFM image showing mosaic twinning in $BaTiO_3$. The sample was etched to

create topographic contrast at the twin boundaries.

Figure 17. Schematic illustration of the (a) $\Sigma5$ and (b) Σ 13 coincident site lattice

geometries. The black points belong to one lattice and the open circles to the other. The

squares denote the repeat unit.

Figure 18. Schematic of the interfacial equilibrium at the point where phase B meets

three grains of phase A. The dihedral angle, Ψ, is a measure the relative interfacial

energies.

Figure 19. Montage of topographic AFM images of a WC/Co surface. The surface was

etched in such a way that the WC crystals were attacked preferentially, and they appear

as the darker contrast. The Co matrix has the lightest contrast.

Fig. 20. SEM image of Ta_2O_5 doped with 3 wt% Al_2O_3 and 1.5 wt% La_2O_3. The dark

grains are Al-rich and the anisotropic grains are a La-rich phase. Micrograph courtesy of

Suxing Wu, Helen M. Chan, and Martin P. Harmer, Department of Materials Science and

Engineering, Lehigh University.

Figure 21. (a) A dendrite observed on the surface an Al-4.5wt% Cu casting. (b) A

section through the same casting, illustrating the appearance of random sections through

the network of Al dendrites. The dark contrast is the Cu rich phase.

Figure 22. (a) transverse and (b) lateral sections through a directionally solidified Ni alloy. The transverse section shows the shape of the primary dendrite while the lateral section shows the arm spacing.

Figure 23. Schematic binary alloy phase diagram.

Figure 24. (a) Schematic of interface instability by constitutional supercooling. As solute is rejected from the solidifying crystal, it accumulates in the valleys between the dendritic protrusions (the solute concentration is indicated by the shading). Since the relatively more pure liquid at the ends of the protrusions freezes at a higher temperature, these portions of the solid grow faster. (b and c) In situ laser confocal microscope image of a solidification front in Fe-Co-Ni alloy at 1597°C. (b) the front is planar (c) a few seconds later, an instability develops. Micrograph courtesy of Chanjoon Paek and Sridhar Seetharaman, Department of Materials Science and Engineering, Carnegie Mellon University.

Figure 25. Light microscope images of the microstructure of directionally solidified (a) CoO-ZrO_2 and (b) NiO-ZrO_2 eutectic microstructures. The darker phase is ZrO_2 and the lighter phase is CoO in (a) and NiO in (b). Micrographs courtesy of Nasim Alem and Vinayak P. Dravid, Department of Materials Science and Engineering, Northwestern University.

Figure 26. Schematic of the growth of a lamellar microstructure maintaining a nearly planar growth front.

Figure 27. Focused Ion Beam microscope image of cuboidal γ' precipitates in a $Ni_{70}Cr_{20}Al_{10}$ superalloy. Micrograph courtesy of Dr. Michael Uchic, Wright Patterson Air

Force Base, and Marc De Graef, Department of Materials Science and Engineering, Carnegie Mellon University.

Figure 28. Schematic image illustrating the difference between (a) a disordered AB alloy and (b) and ordered arrangement with and antiphase domain boundary.

Figure 29. The transmission electron micrograph of Fe 55 at.%Pd alloy annealed at 400 °C for 140 h. The micrograph shows the antiphase domains and antiphase boundaries (APBs) formed during the atomic ordering process. Micrograph courtesy of Lisha Wang and David. E. Laughlin, Department of Materials Science and Engineering, Carnegie Mellon University.

Figure 1. G.S. Rohrer

20 μm
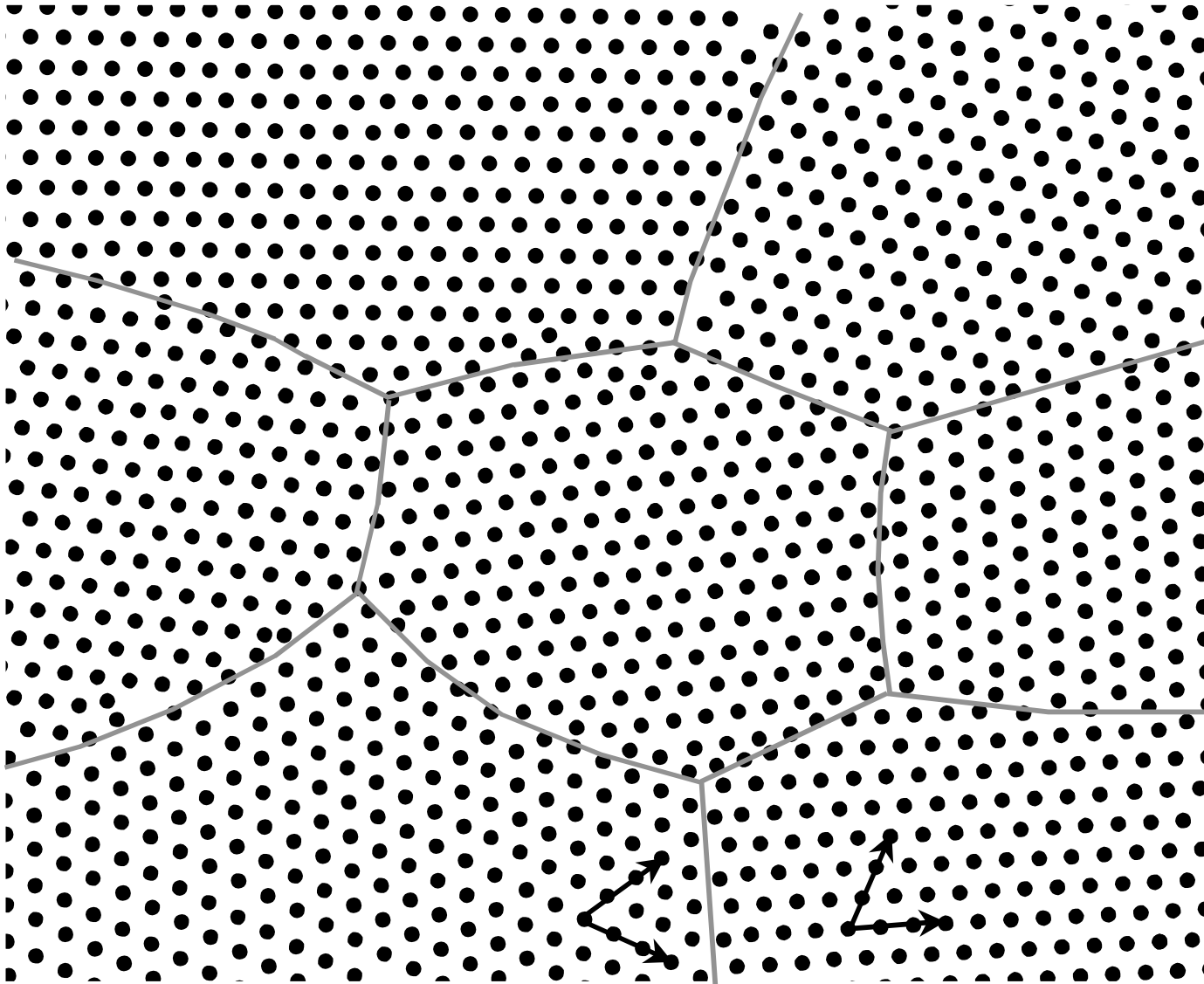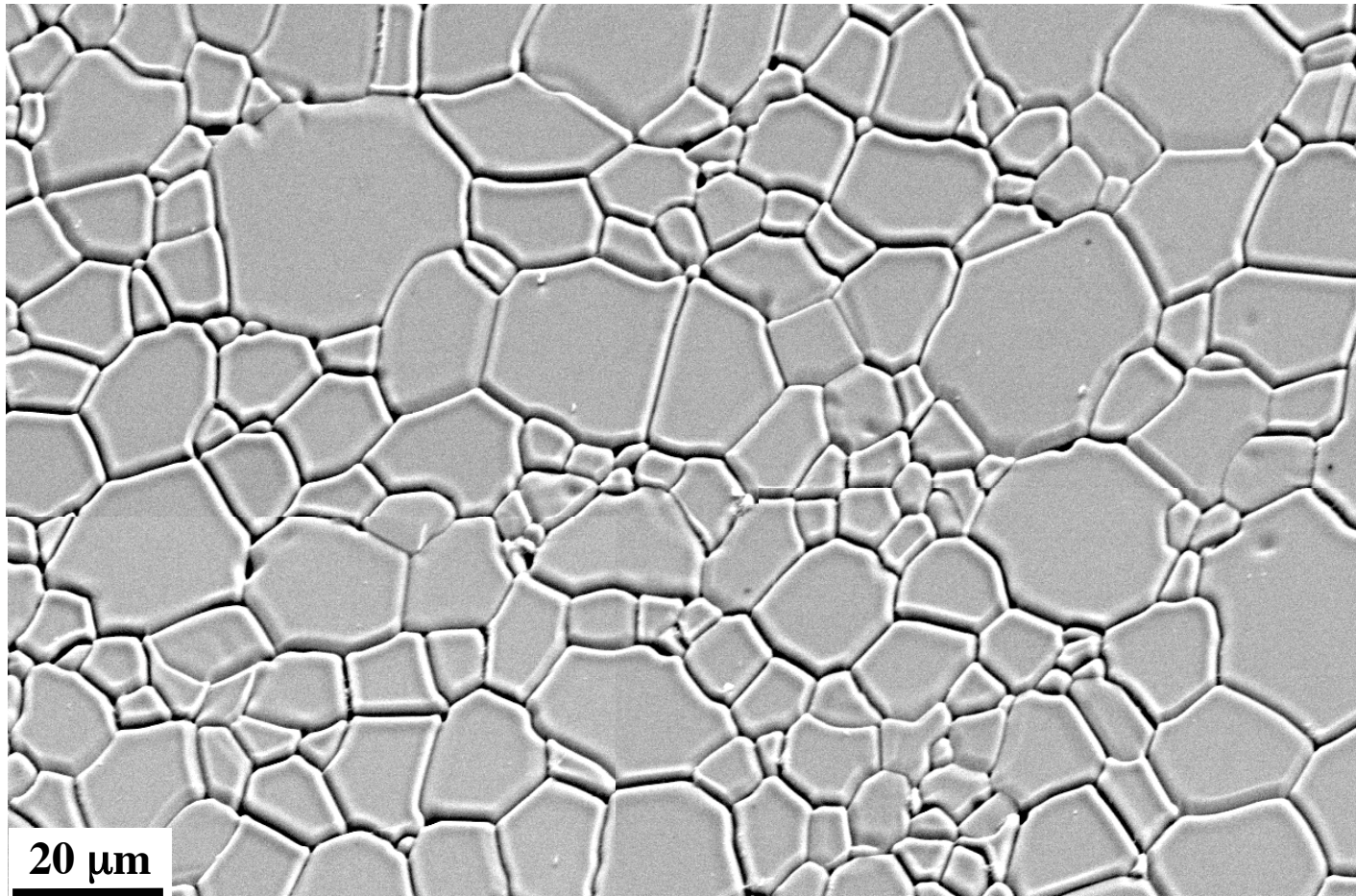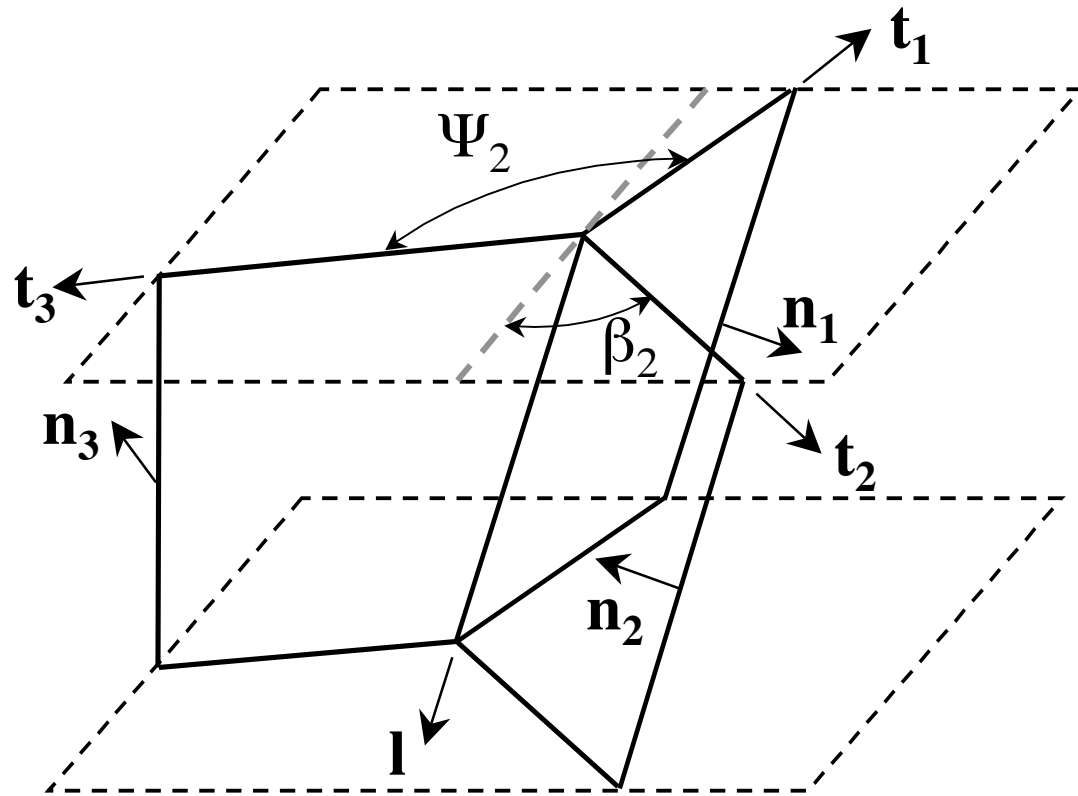
Figure 2. G.S. Rohrer

Figure 3. G.S. Rohrer
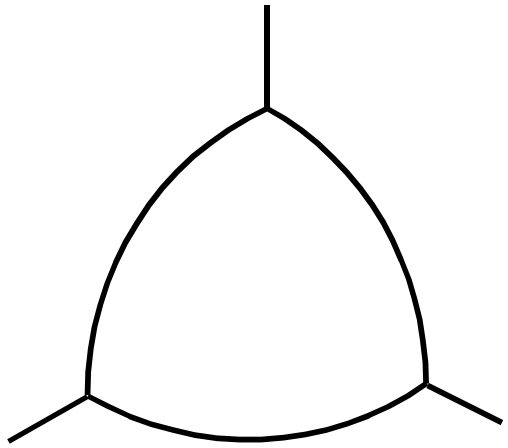
(a)
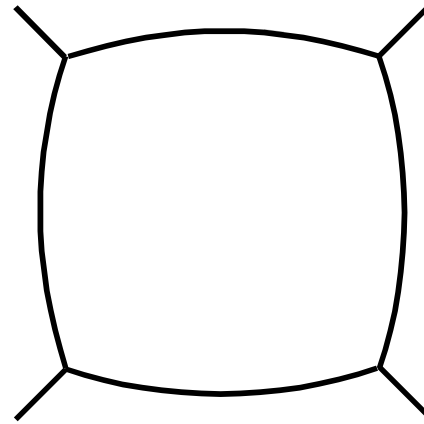
(b)
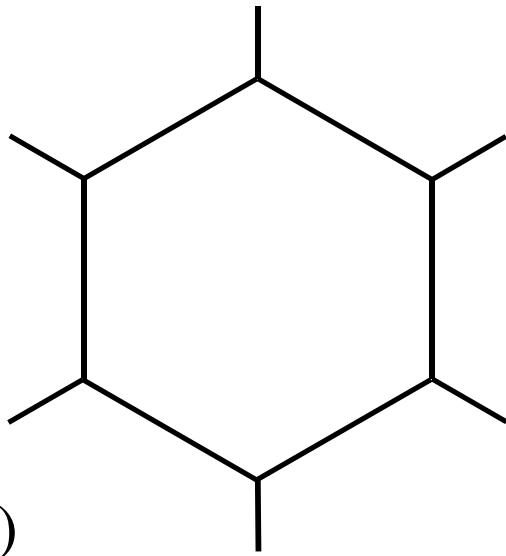
(c)
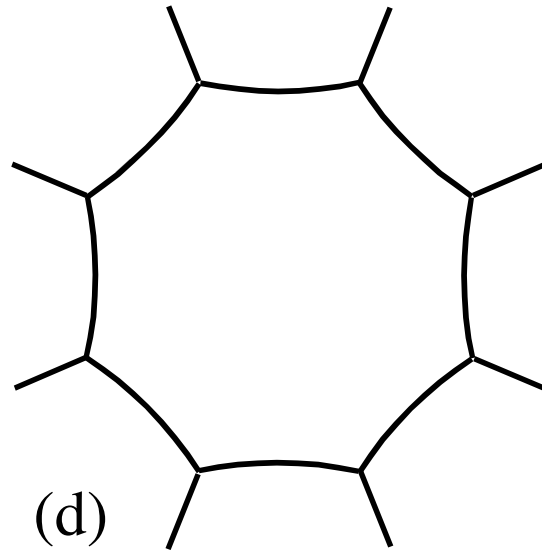
(d)

Figure 4. G.S. Rohrer
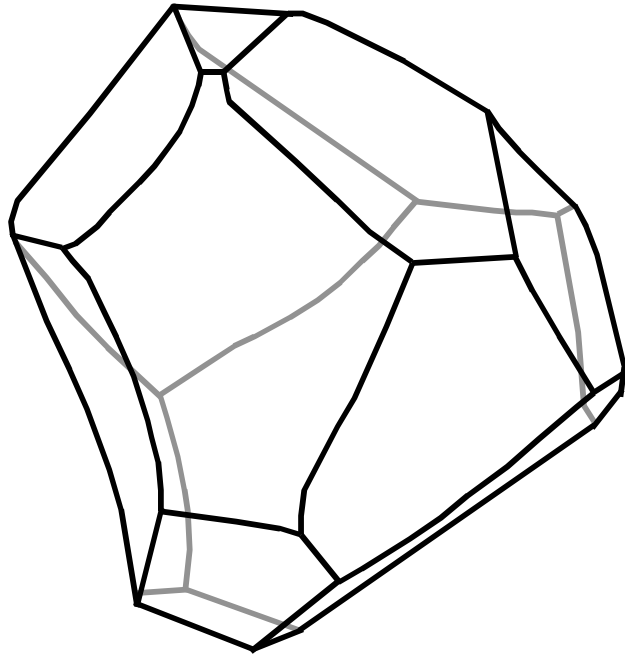
Figure 5. G.S. Rohrer
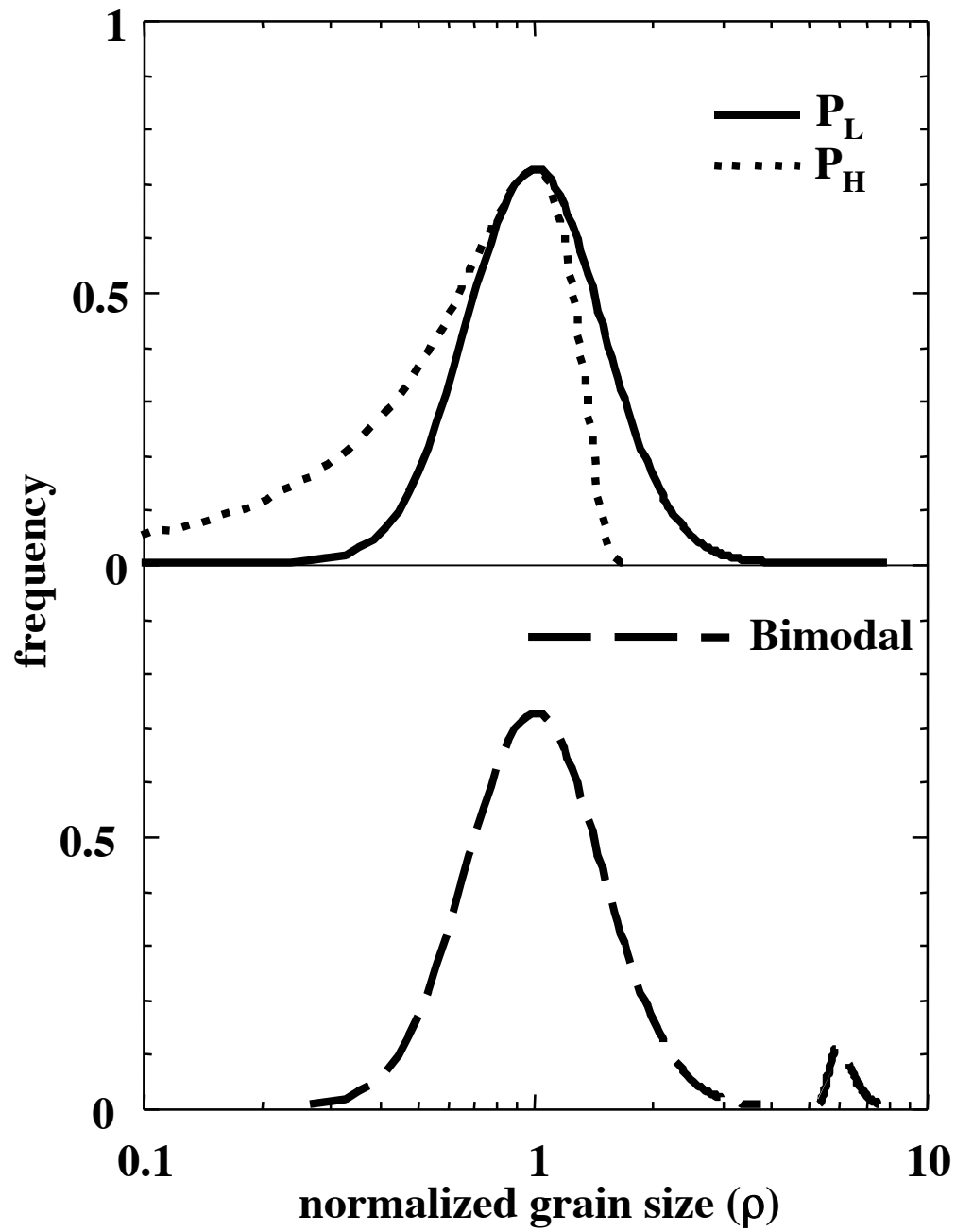
Figure 6. G.S. Rohrer
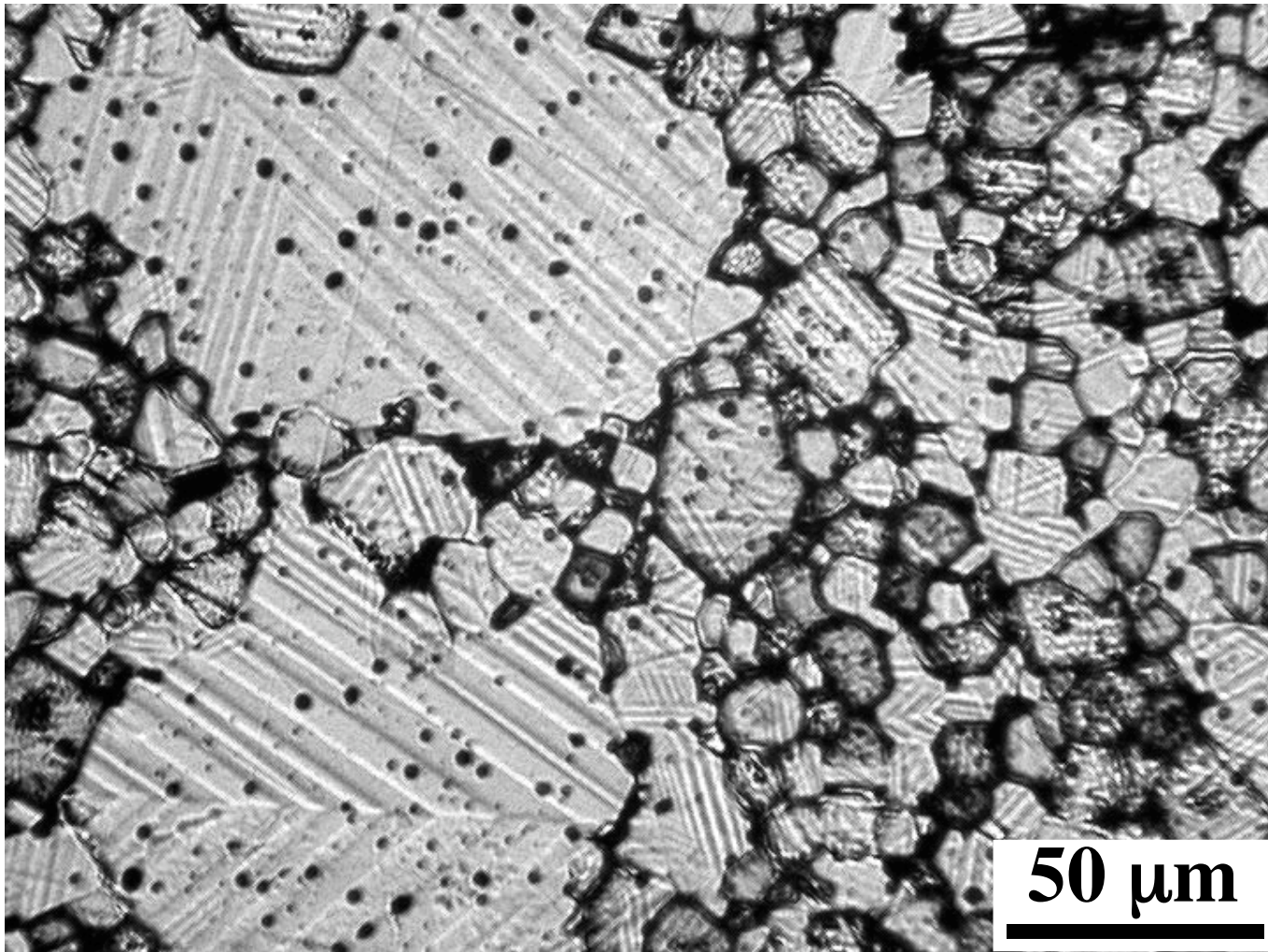
Figure 7. G.S. Rohrer
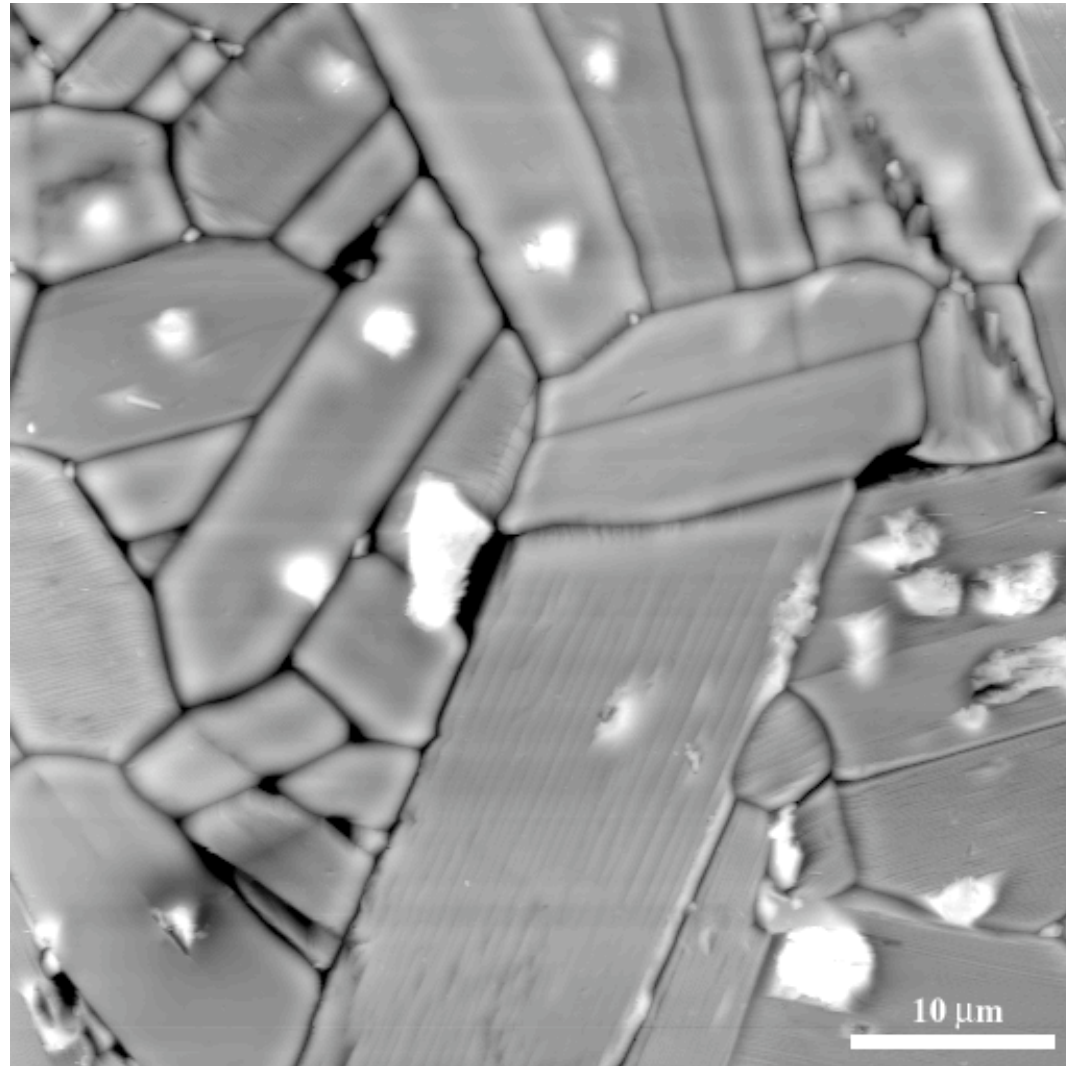
Figure 8. G.S. Rohrer
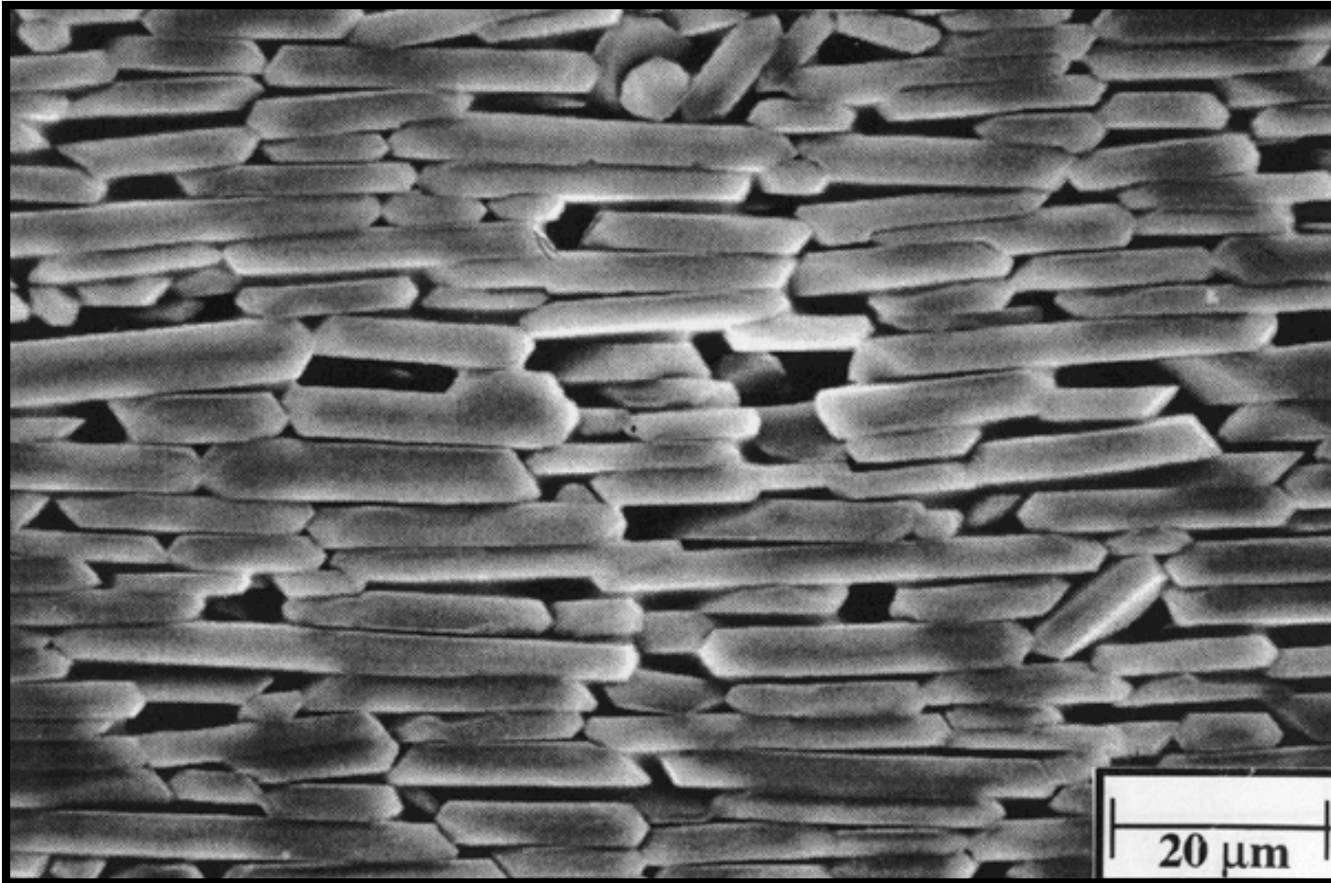
Figure 9. G.S. Rohrer
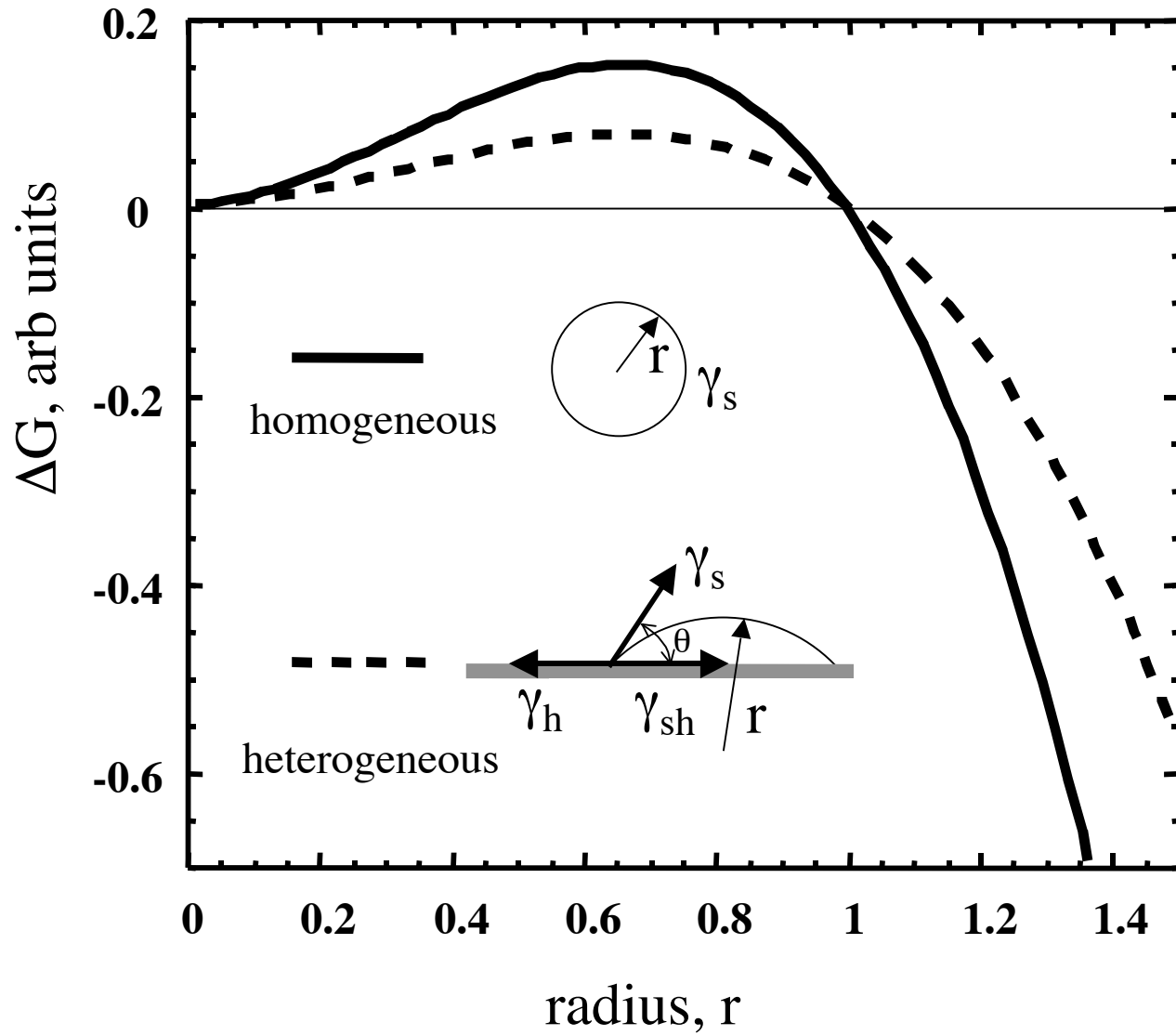
Figure 10. G.S. Rohrer

Figure 11. G.S. Rohrer

10 nm

Co alloy (HCP)

Cr alloy

NiAl

Ni-P plated layer

60 nm
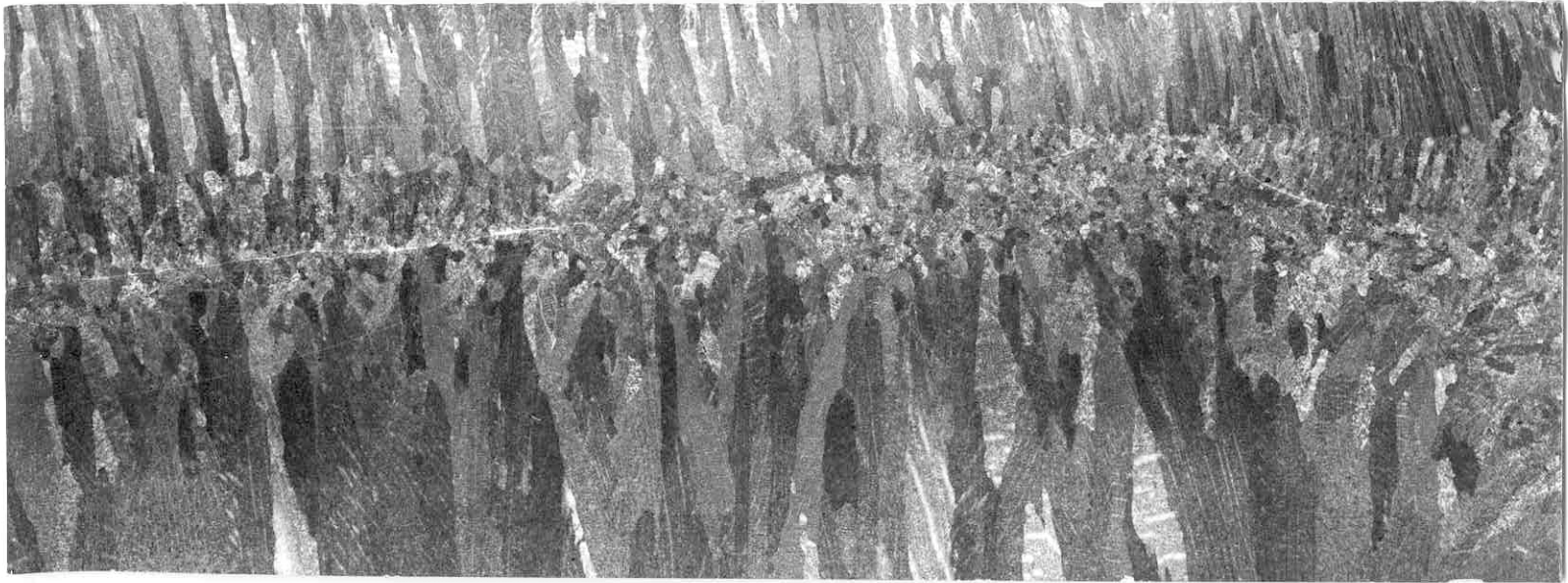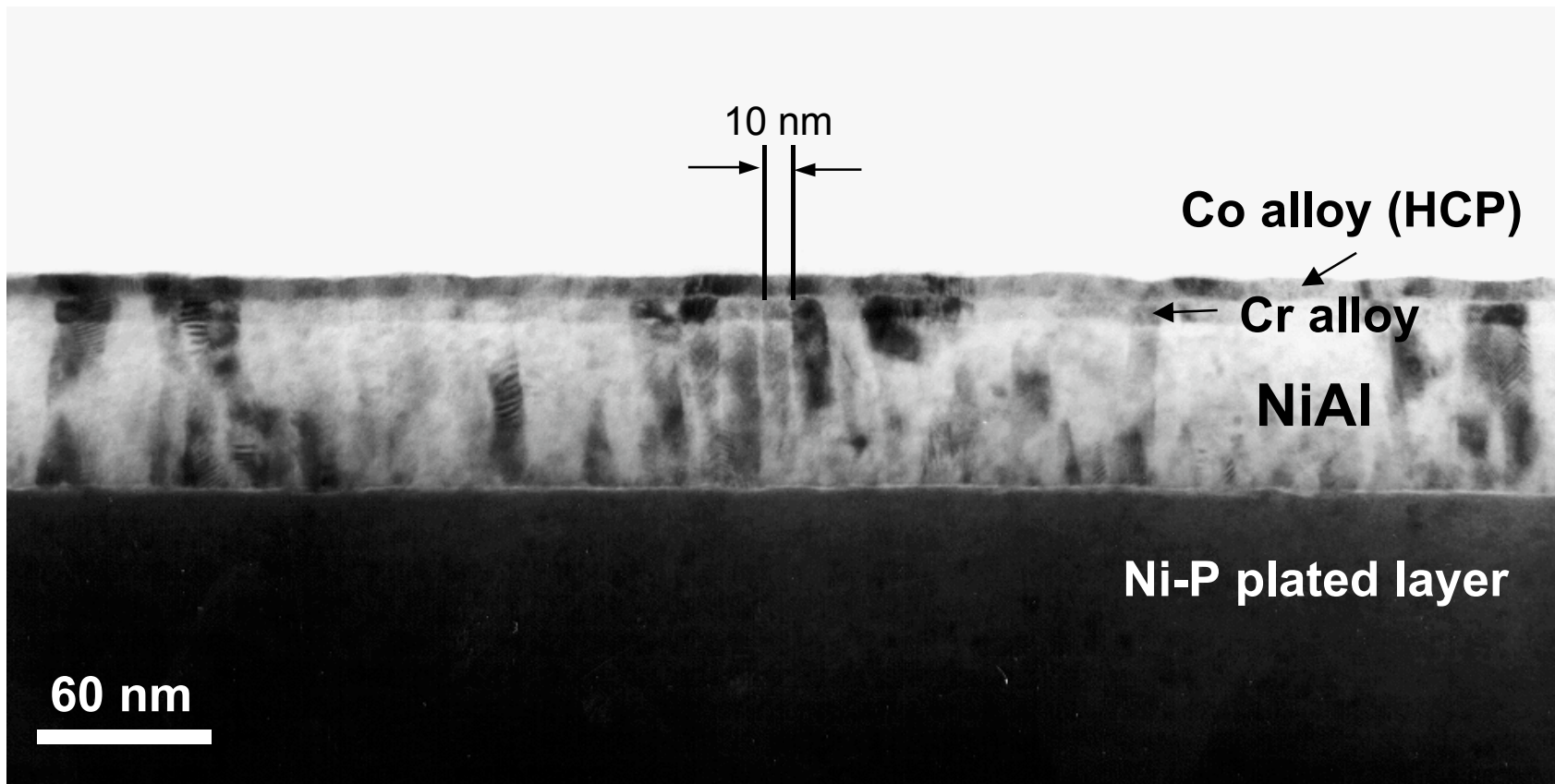
Figure 12. G.S. Rohrer

Figure 13. G.S. Rohrer

MRD

	158.00
	142.20
	126.40
	110.60
	94.80
	79.00
	63.20
	47.40
	31.60
	15.80
	0.00

MRD

	19.70
	17.78
	15.86
	13.94
	12.02
	10.10
	8.18
	6.26
	4.34
	2.42
	0.50

(a)

(b)
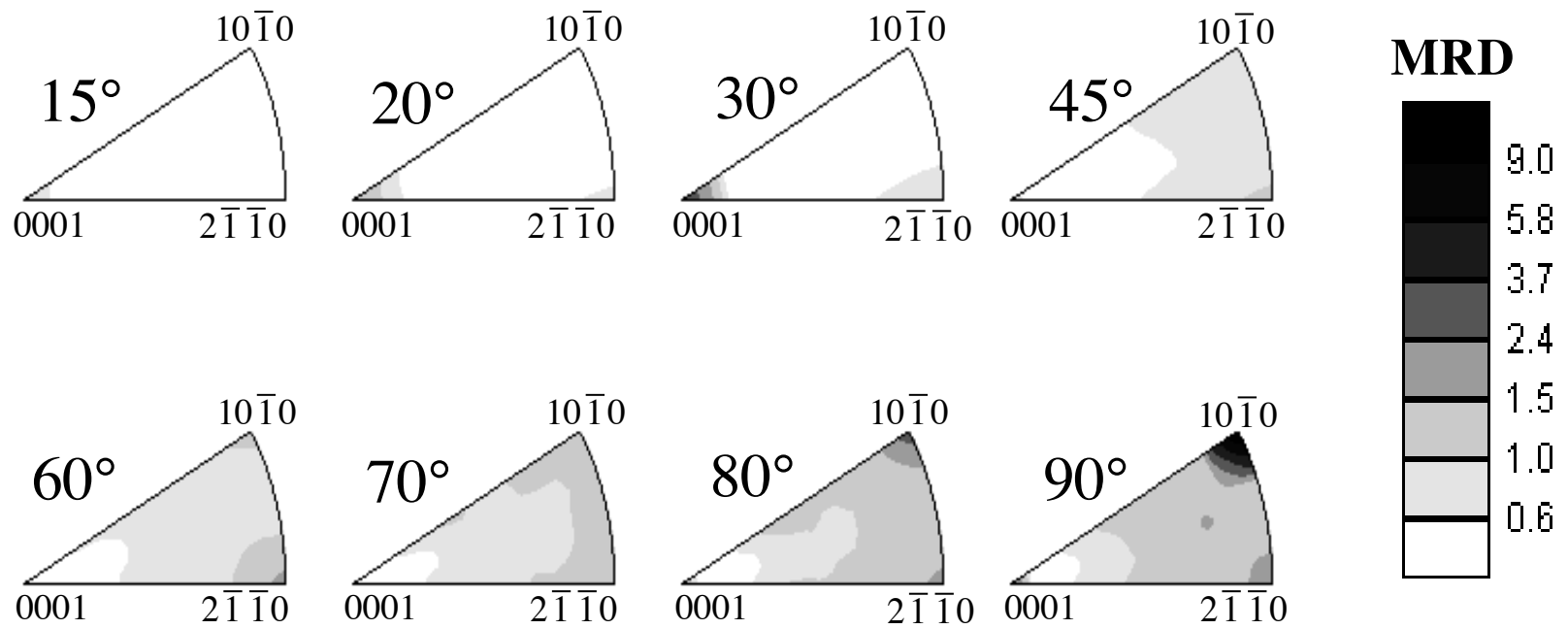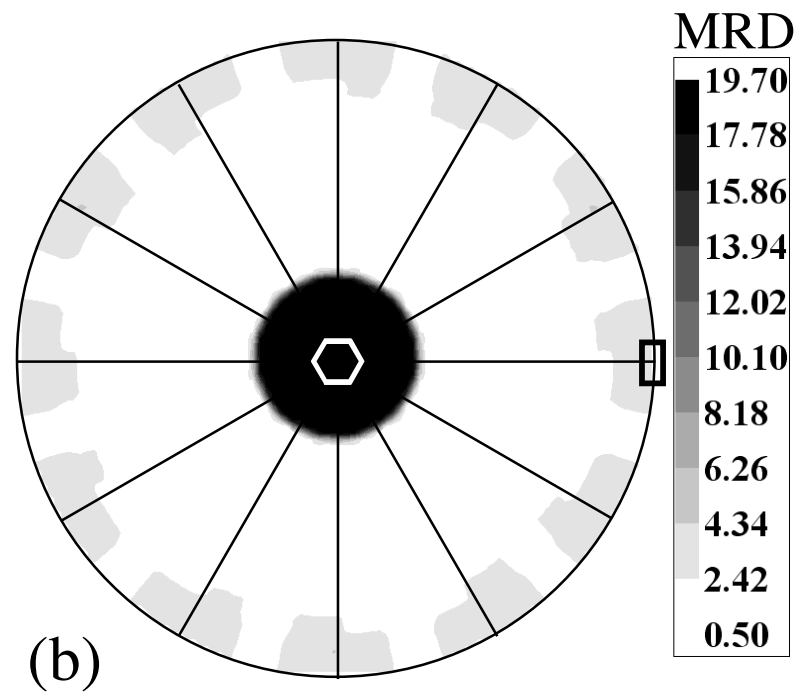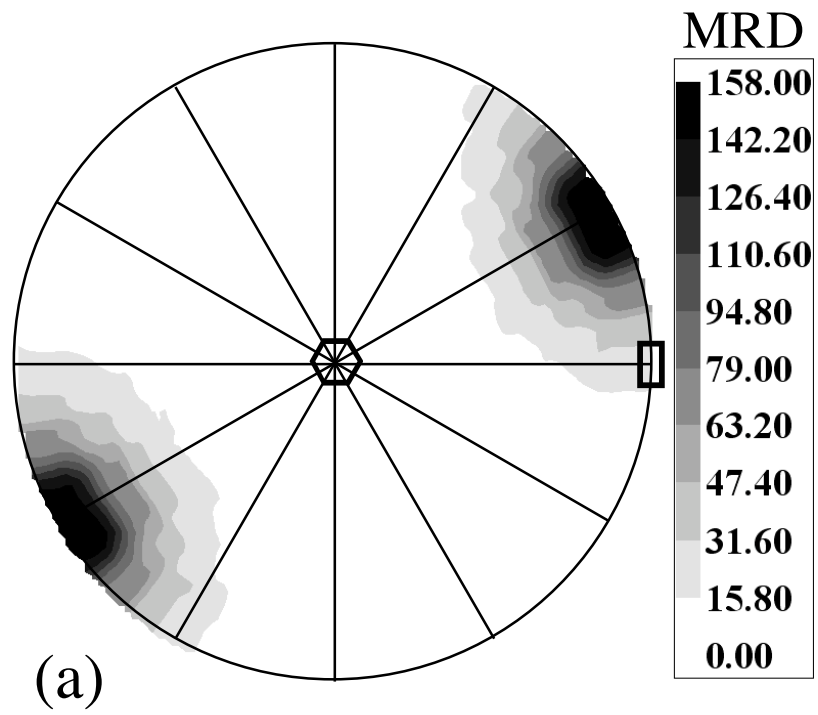
Figure 14. G.S. Rohrer

250 μm
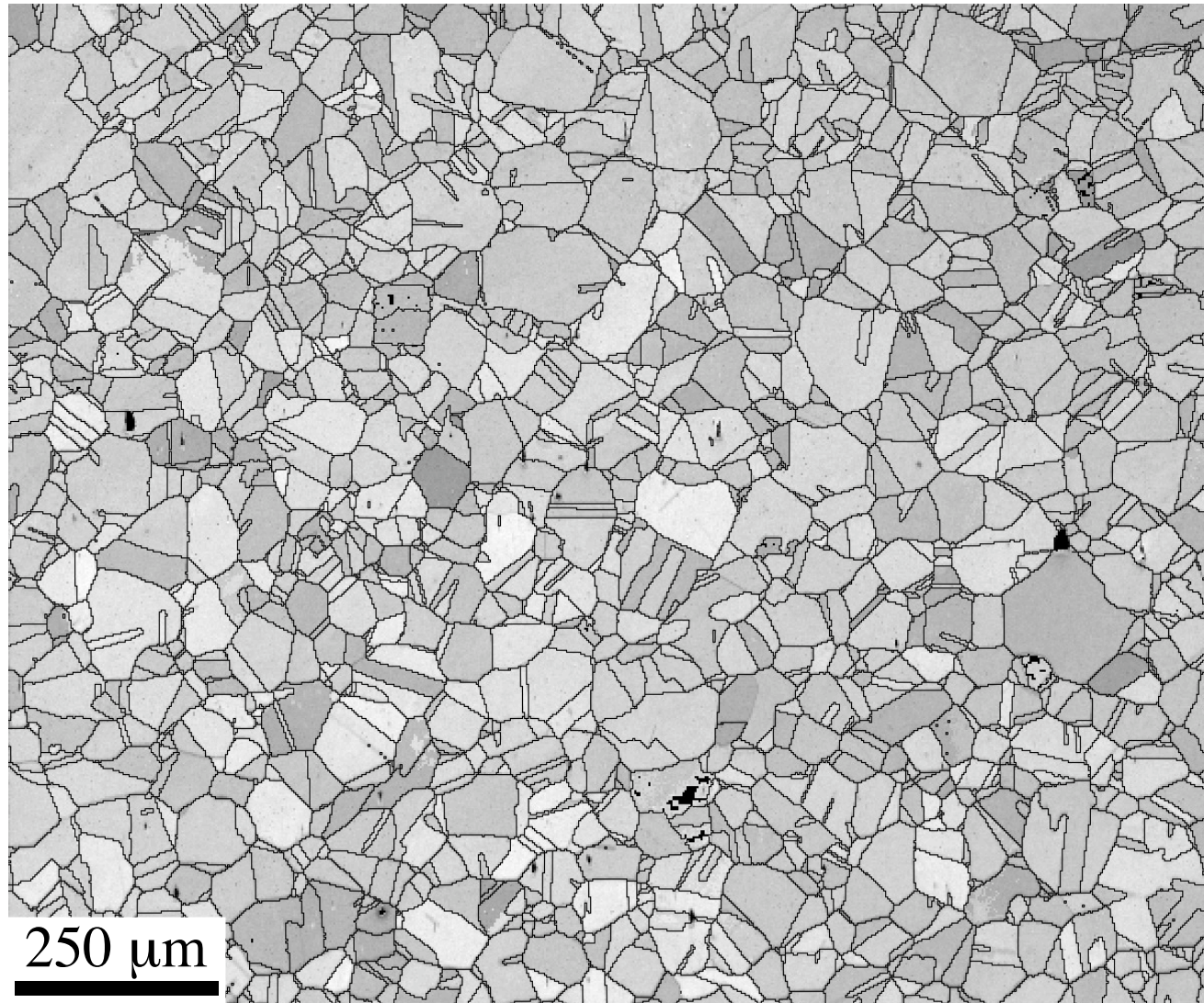
Figure 15. G.S. Rohrer

3 μm
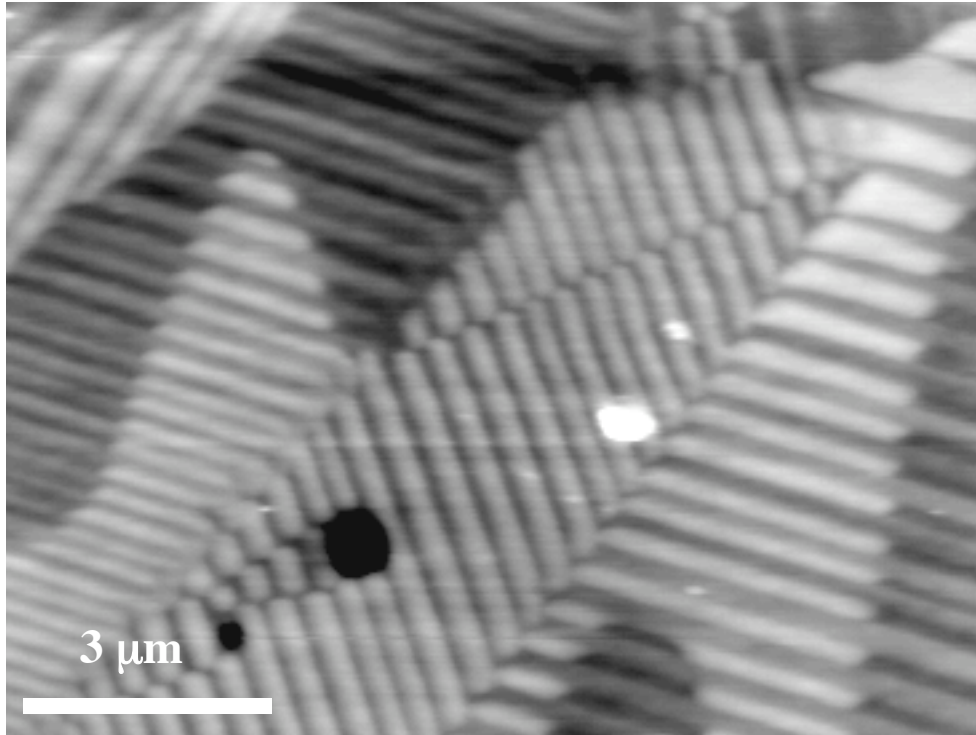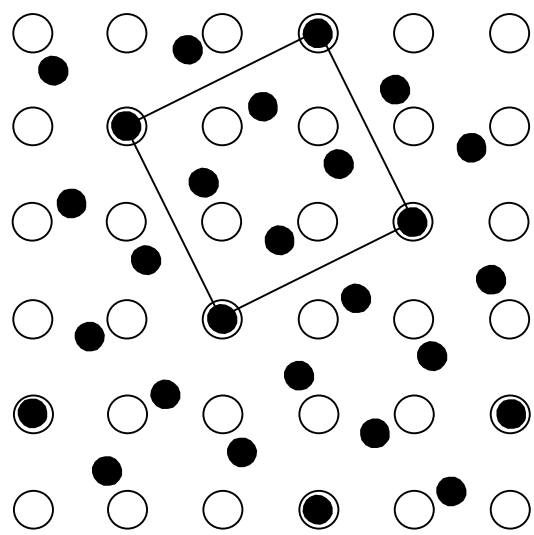
Figure 16. G.S. Rohrer
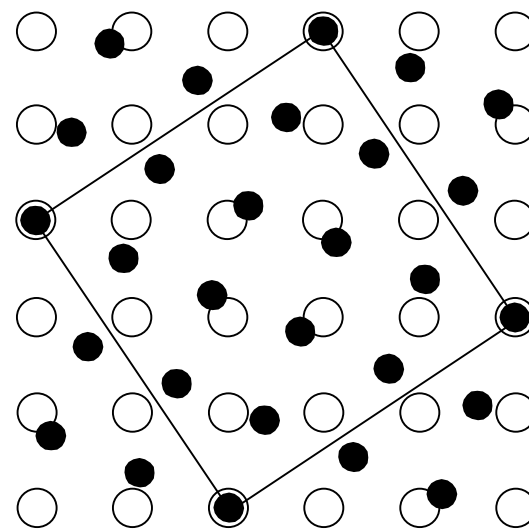
(a)   (b)

Figure 17. G.S. Rohrer
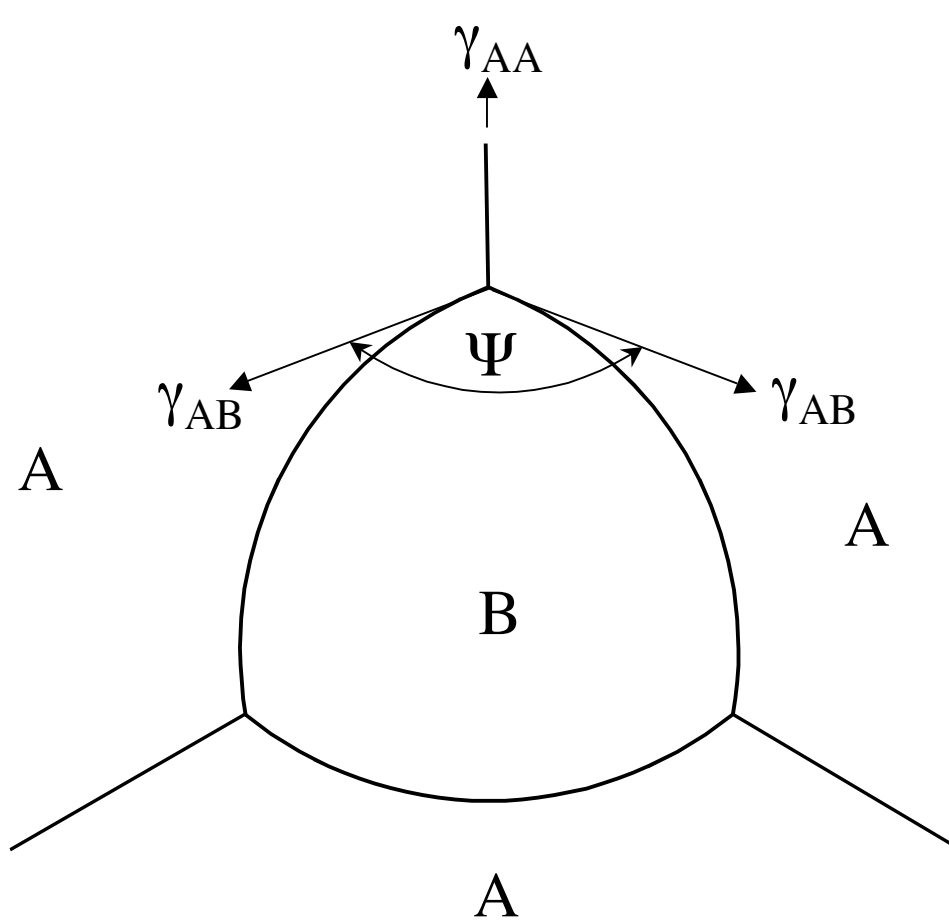
Figure 18. G.S. Rohrer

50 μm
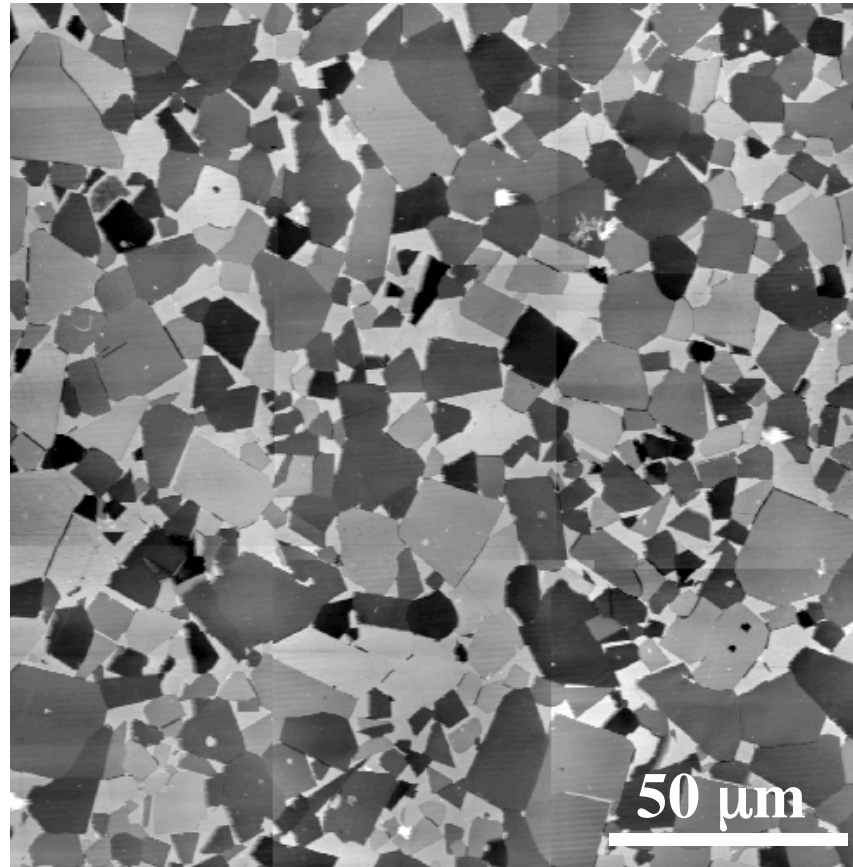
Figure 19. G.S. Rohrer
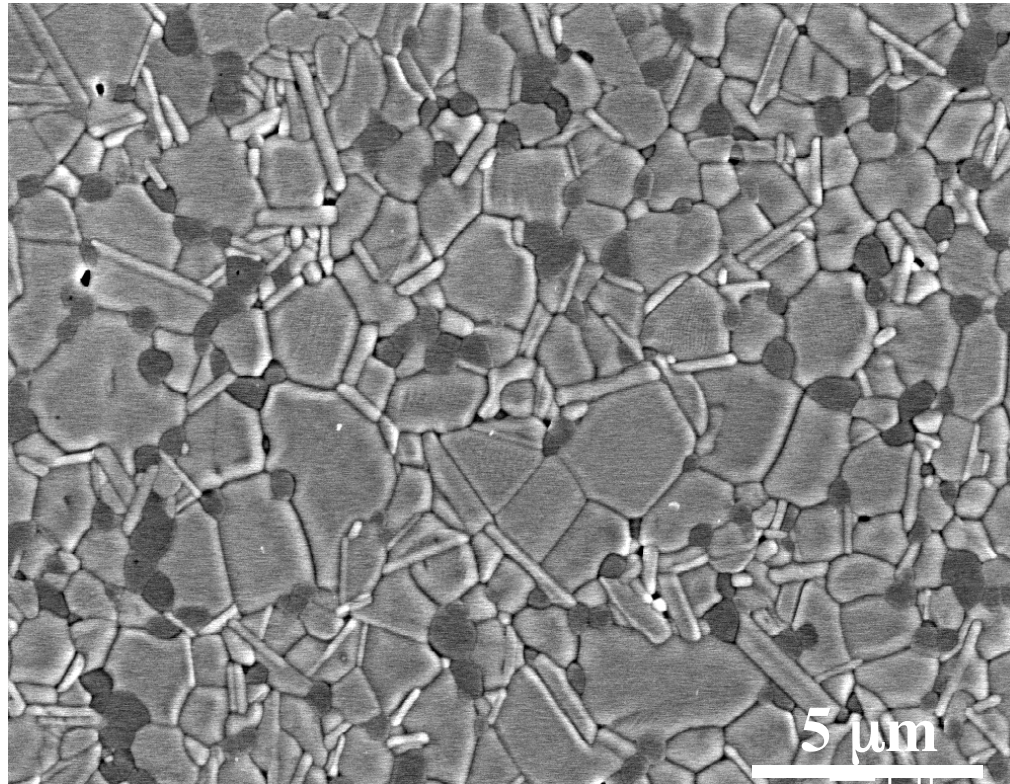
Figure 20. G.S. Rohrer
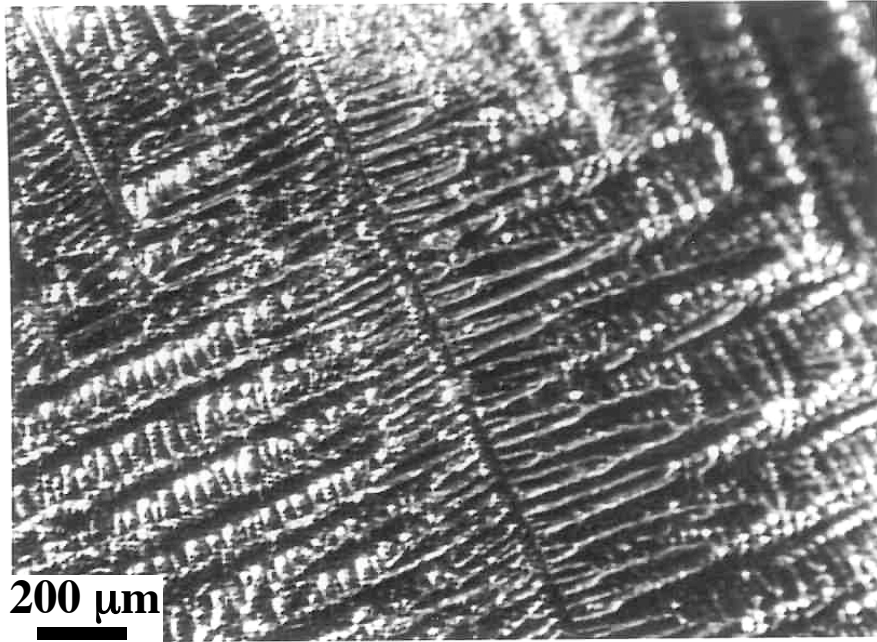
(a)
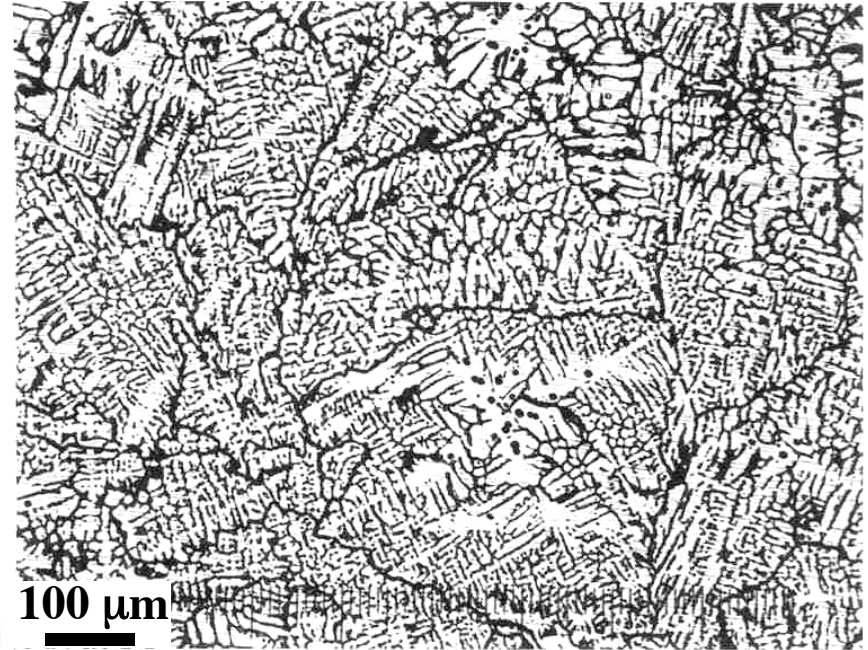
(b)

Figure 21. G.S. Rohrer

100 μm

(a)

100 μm
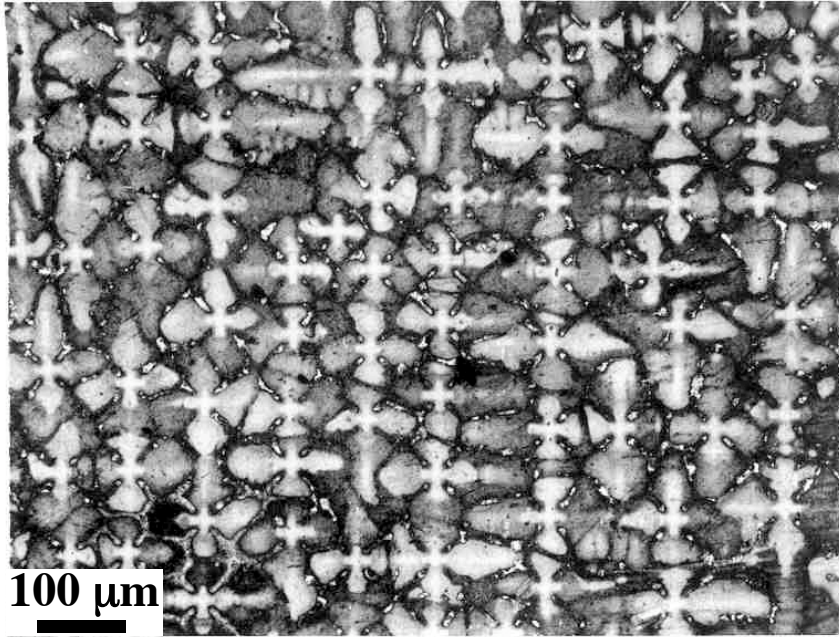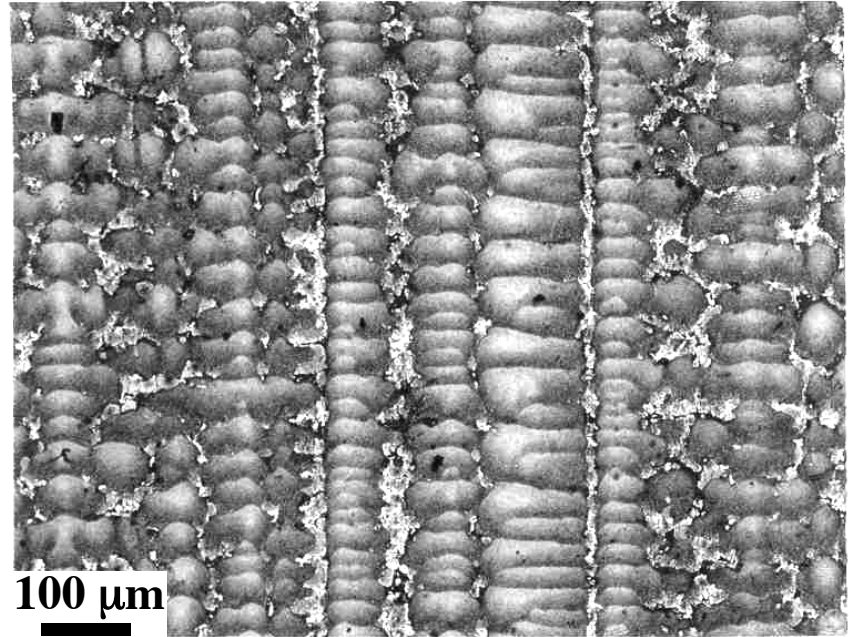
(b)

Figure 22. G.S. Rohrer
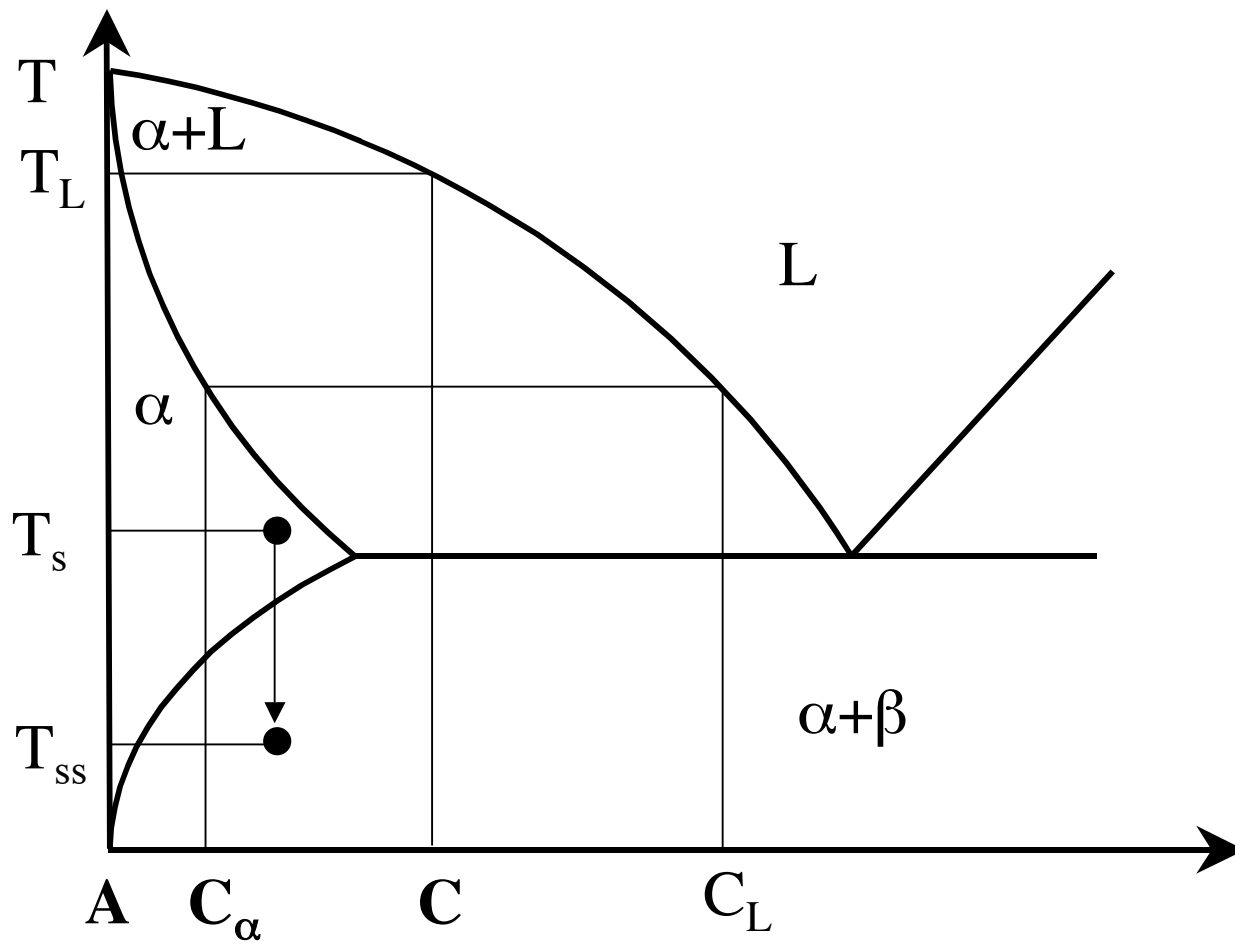
Figure 23. G.S. Rohrer

(a)

(b)   70 μm

(c)   70 μm
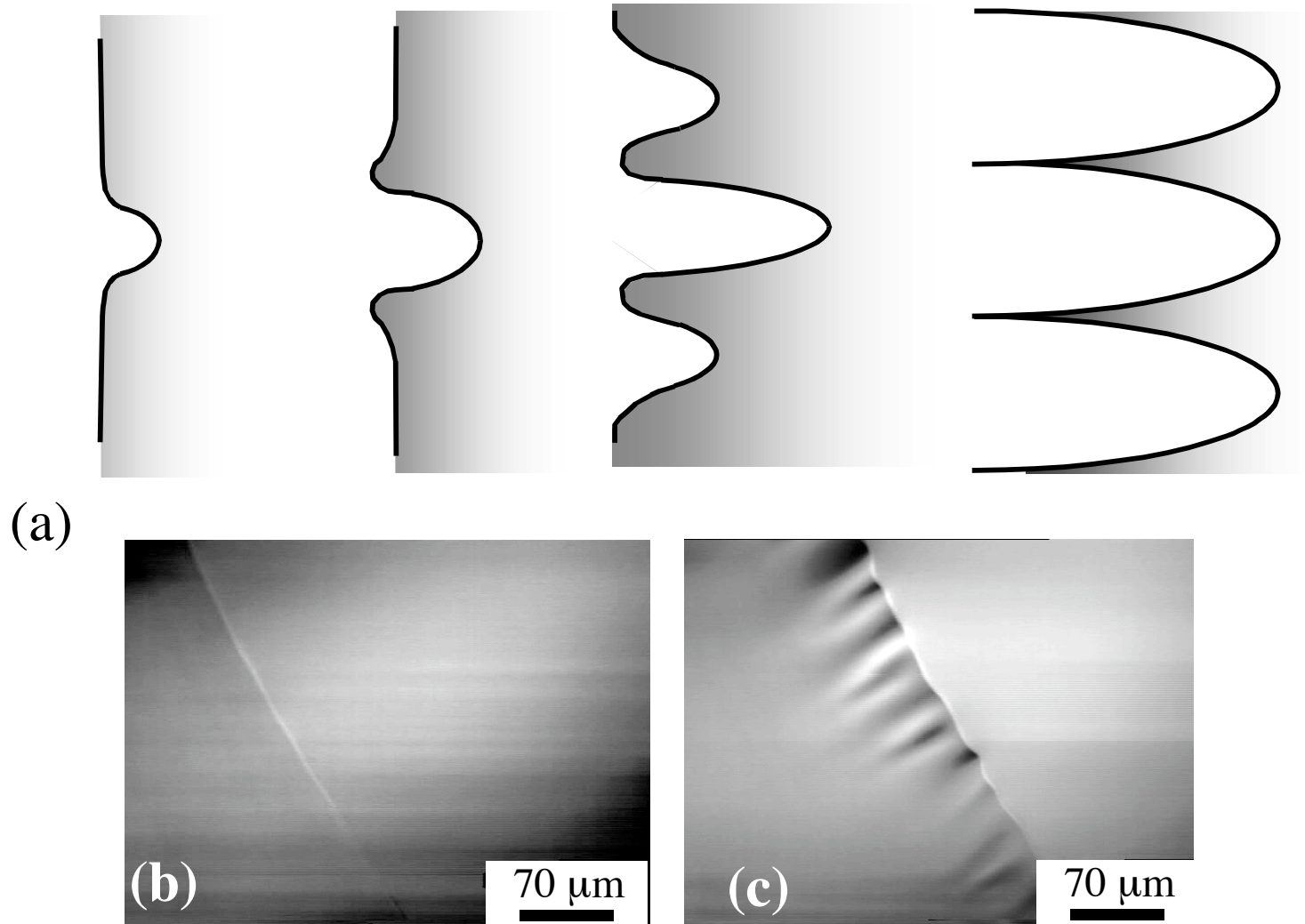
Figure 24. G.S. Rohrer
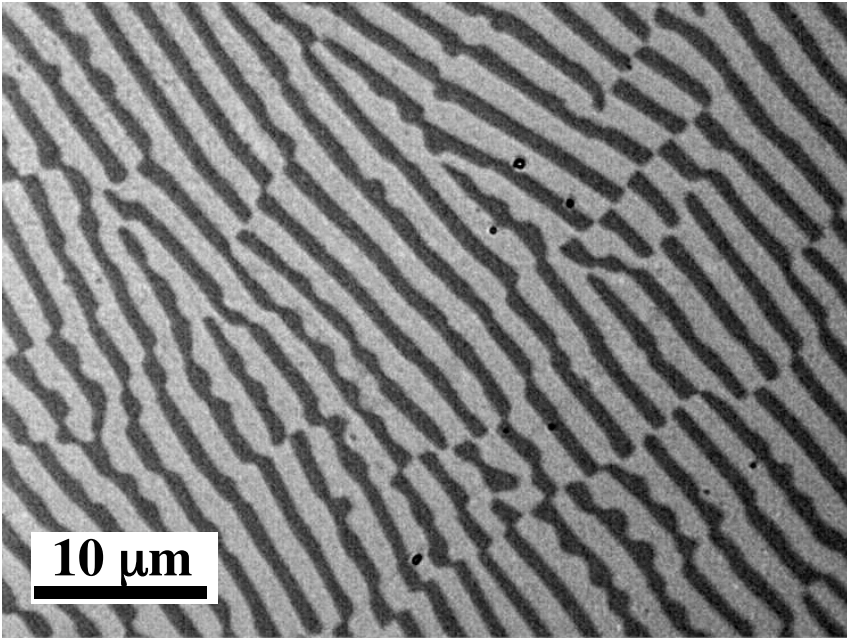
(a)
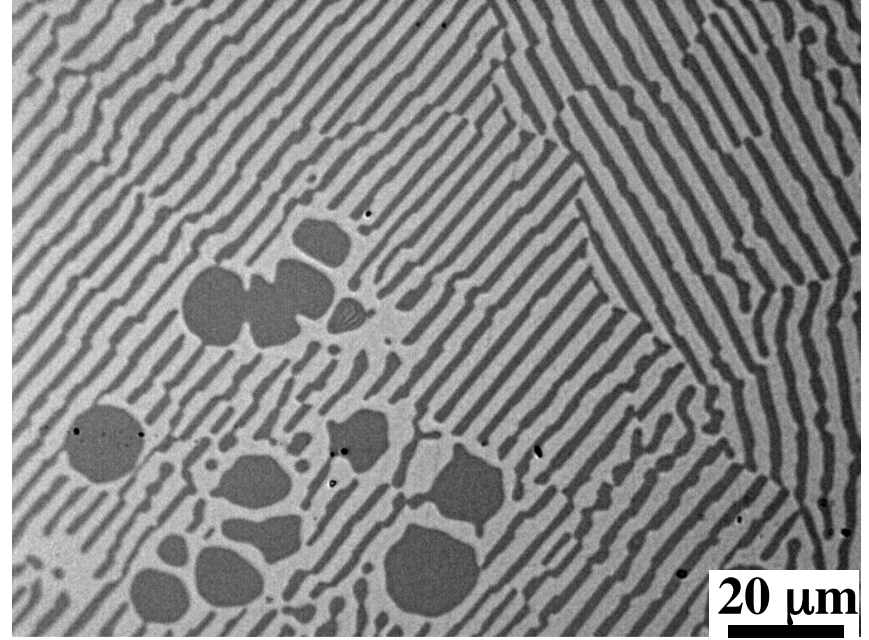
(b)

Figure 25. G.S. Rohrer

α

β

A

B

Liquid

α

A

β
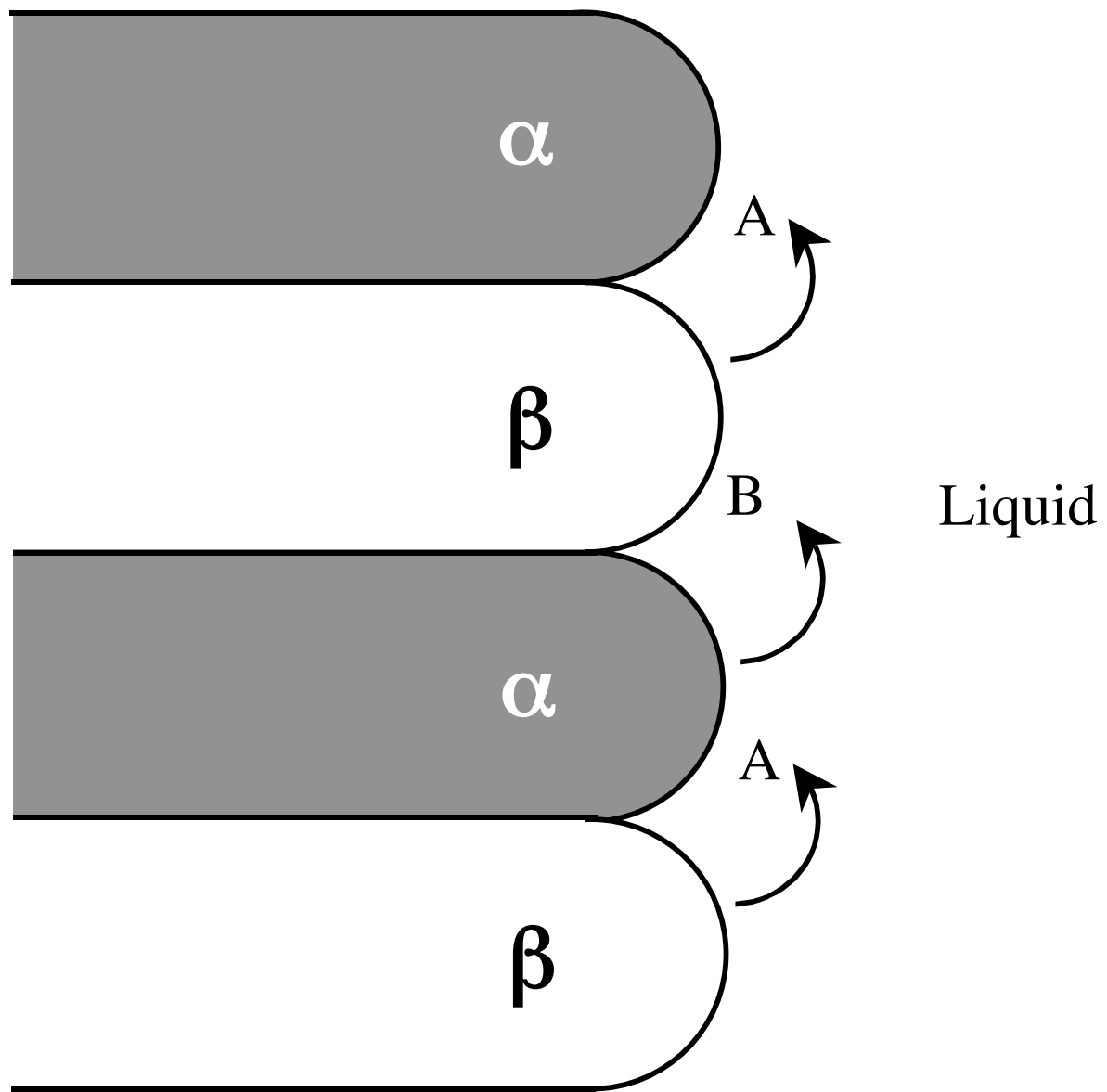
Figure 26. G.S. Rohrer
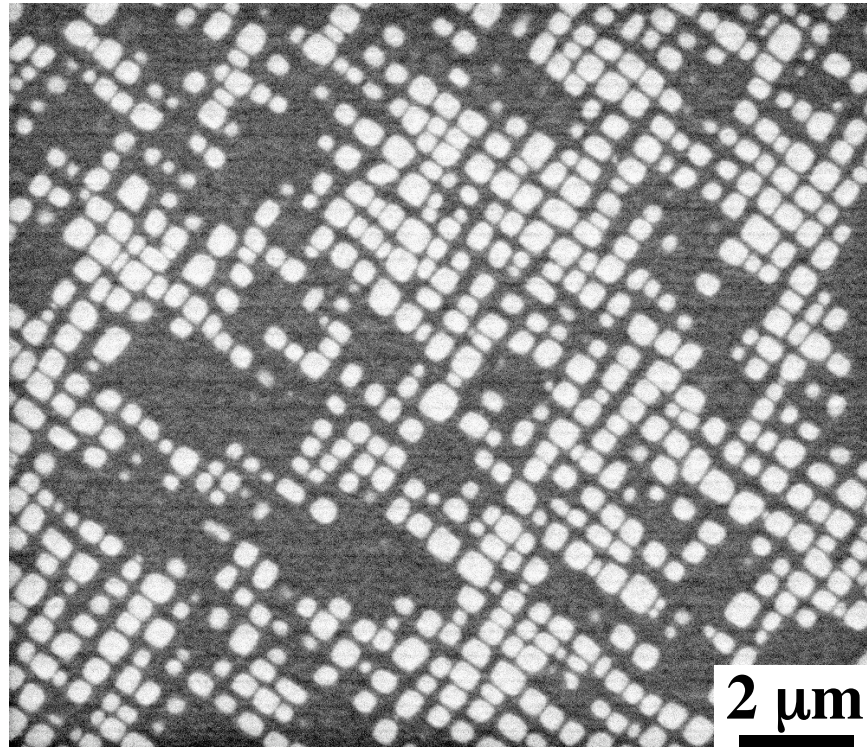
Figure 27. G.S. Rohrer

APB
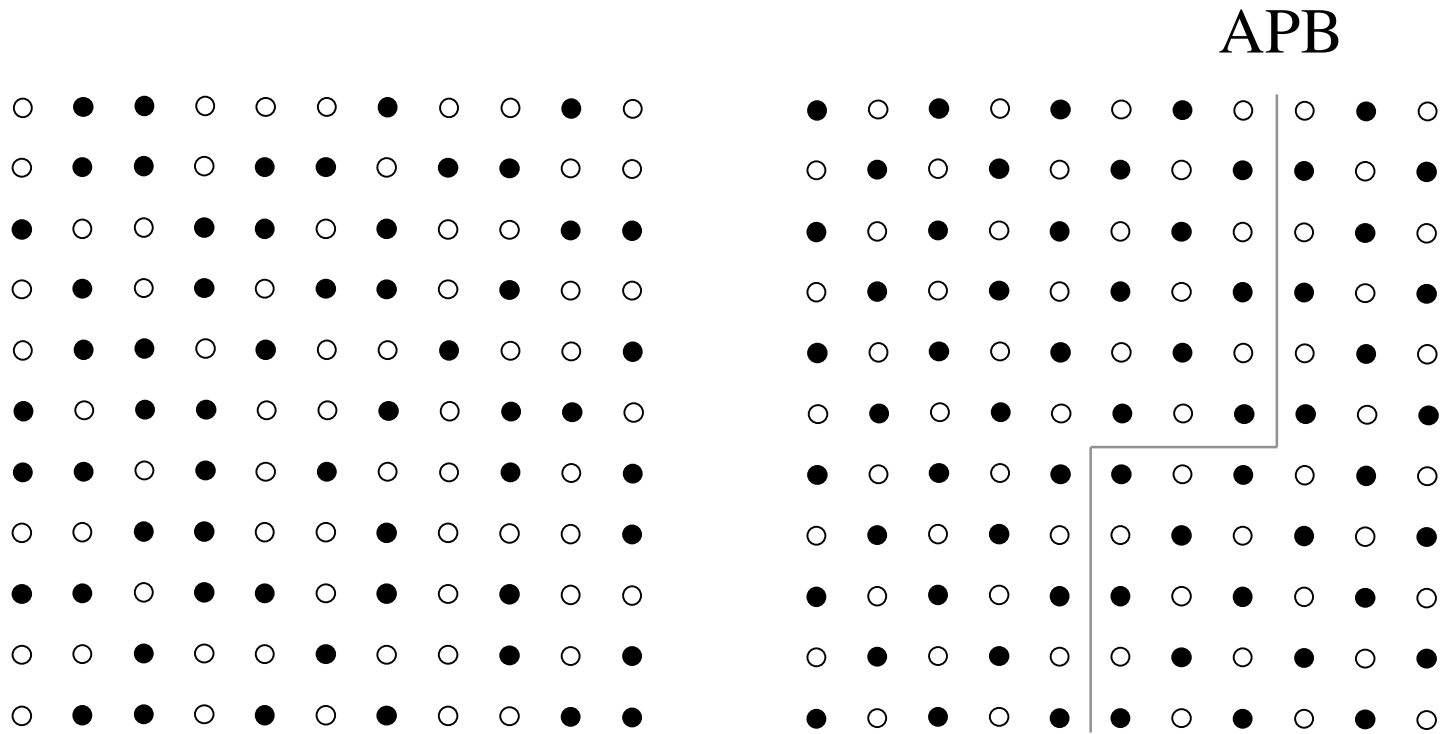
Figure 28. G.S. Rohrer

Figure 29. G.S. Rohrer